CENTRO DE INVESTIGACIÓN Y DE ESTUDIOS AVANZADOS DEL
INSTITUTO POLITÉCTINO NACIONAL

Restrictions to Lorentz invariance violation by cosmic and gamma rays

by

Humberto Martínez Huerta

A thesis submitted in partial fulfillment for the degree of
Doctor in Science with the specialty in Physics

in the

Physics Department

Advisor

Dr. Abdel Pérez Lorenzana

March, 2017

Resumen

Los escenarios astrofísicos ofrecen una oportunidad única para buscar posibles señales de nueva física debido a las altas energías y a las largas distancias que ellas implican. Entre estas señales, se encuentran las motivadas por violación a la invariancia de Lorentz. Bajo este espíritu, en este trabajo introducimos la violación de invariancia de Lorentz como una modificación genérica de las relaciones de dispersión de partículas con el fin de estudiar procesos de atenuación en rayos cósmicos y gamma de muy alta energía. Mostramos que la corrección isotrópica a la relación de dispersión de fotones por violación hipotética de invariancia de Lorentz, reproduce los mismos efectos físicos, para el proceso de radiación Cherenkov en el vacío, que algunos modelos particulares con ruptura espontánea de la simetría de Lorentz. Mostramos también que éste proceso exhibe un comportamiento sensible a la masa y carga del rayo cósmico primario. La aproximación que hemos desarrollado en este trabajo la aplicamos también en el estudio de la desintegración de fotones en el vacío por violación a la simetría de Lorentz y mostramos que aquellos fotones con energía suficientemente alta decaen muy rápido, por lo que hemos derivado límites estrictos a la escala de violación de Lorentz, por la observación directa de fotones de muy alta energía con telescopios de rayos gamma. Por último, abordamos los procesos de fotoproducción mediante interacción con rayos cósmicos y gammas con el fondo difuso de fotones, y demostramos que la violación de Lorentz puede, además de generar desplazamientos en la energía umbral de producción, suprimir el proceso de atenuación a energías superiores a un segundo umbral bien definido.

Abstract

Astrophysical scenarios provide a unique opportunity to test the possible signatures of Lorentz invariance violations due to the high energies and the very long distances they involve. Following this spirit, in this work, we have used Lorentz invariance violation introduced as a generic modification to particle dispersion relations to study high energy cosmic ray attenuation processes. It is shown that isotropic correction to the photon dispersion relation by hypothetical Lorentz invariance violation reproduces the same physical effects for vacuum Cherenkov radiation as in some particular models with the spontaneous breaking of Lorentz symmetry. We show that the last process has a dependency on the cosmic ray primary mass and charge. The approximation we have achieved in this work is also implemented to study photon decay in a vacuum. We show that photons of sufficient energy are unstable and decay very fast; hence stringent limits to the violation scale are derived from the direct observation of very high energy cosmic ray photon events on gamma-ray telescopes. Finally, photoproduction processes by cosmic and gamma-ray primaries on photon background are also addressed to show that Lorentz violation may turn off this attenuation process at energies above a well defined secondary threshold, additionally to the expected threshold shift by LIV.

Acknowledgements

I want to express my very great appreciation to my advisor Professor Abdel Pérez Lorenzana. His office's door was always open whenever I needed it, and I am very grateful for that. For his invaluable time, support, and for shaping this thesis, thanks.

My special thanks to my thesis committee members, Professors Nora Eva Bretón Báez, Pablo Roig Garcés, Juan Carlos Arteaga Velázquez and Arnulfo Zepeda Domínguez for their effort, comments and corrections made to this work and thesis.

My special thanks go to Professors Karen Salomé Caballero Mora and Arnulfo Zepeda Domínguez for all the encouragement, support, and advice given in the course of this work and beyond.

Advice, feedback, and enlightening discussions given by Professors James T. Linnemann, J. Patrick Harding, Lukas Nellen, and also the HAWC Collaboration and the Pierre Auger Collaboration, have helped develop this thesis and results.

I also want to offer my special thanks to Prof. Vitor de Souza and the M.Sc Rodrigo Guedes Lang from Instituto de Física de São Carlos, Universidade de São Paulo, for their hospitality and enlightening discussions during my internship in São Carlos, Brazil.

To my family, my mother and brother, I am immensely grateful for their support in the huge and small things, for always be where and when I need them the most, thanks. I will always be grateful to my beloved Alma for all the support, constant motivation, and lovely understanding during this journey. To my friends and colleagues in Cinvestav, Vicente, Isaac, and J. Germán, for the enlightening discussions, feedback, and all the good times during the last four years, thanks.

This work is an effort in which, directly or indirectly, many people participated, and I am very grateful to them: friends, teachers, colleagues, the Red Estudiantil Cinvestav (REC), etc. To all of them, no less important to me, and whose names I would not finish enlisting here, a vast and profound thanks.

Finally, I acknowledge the financial support from the Consejo de Ciencia y Tecnología (Conacyt) for grant 243119 from September 1st, 2012 to August 31st, 2016. This work was also partially supported by grants 132197 and 237004. I am grateful to the Centro de Investigación y Estudios Avanzados del Instituto Politécnico Nacional (Cinvestav) for the support and facilities given to me in the development of this work, and I would like to extend my special thanks to all the staff in Cinvestav, especially for the people in the Physics Department, whose work and dedication I really appreciate.

Contents

Abbreviations

LI	**L**orentz **I**nvariance
LIV	**L**orentz **I**nvariance **V**iolation
SM	**S**tandard **M**odel
SME	**S**tandard **M**odel **E**xtension
mSME	**m**inimal **S**tandard **M**odel **E**xtension
QFT	**Q**uantum **F**ield **T**heory
QG	**Q**uantum **G**rativy
GR	**G**eneral **R**elativity
SR	**S**pecial **R**elativity
modM	**mod**ified **M**axwell
MCS	**M**axwell **C**hern **S**imons
LIVgen1	**L**orentz **I**nvariance **V**iolation **gen**eric approach at leading order in α_n
VHE	**V**ery **H**igh **E**nergy
CR	**C**osmic **R**ays
UHECR	**U**ltra **H**igh **E**nergy **C**osmic **R**ays
GZK	**G**reisen **Z**atsepin **K**uz'min
PAO	**P**ierre **A**uger **O**bservatory
HESS	**H**igh **E**nergy **S**tereoscopic **S**ystem
HEGRA	**H**ight **E**nergy **G**amma **R**ay **A**stronomy
HAWC	**H**igh **A**ltitude **W**ater **C**herenkov
SNR	**S**upernova **R**emnants
EAS	**E**xtensive **A**ir **S**hower

To my father,

who always knew what I am
starting to understand . . .

Humberto R. Martínez Ávila

(1959-1990)

Chapter 1

Introduction

Lorentz symmetry stands as one of the cornerstones of fundamental physics. Nonetheless, as for any other fundamental principle, exploring its limits of validity, has been an important motivation for theoretical and experimental research on the past [1]. Currently, supported models with Lorentz invariance violation (LIV) have renewed the interest of the community due to the opportunity to observe or restrict new physics with the recent measurements from the Observatories at the highest energies.

Lorentz invariance violation is motivated as a possible consequence of beyond the standard model (SM) theories, such as quantum gravity or string theory, just to mention some (see for instance Refs. [1–10]). However, the lack of observations of the LIV derived phenomena imposes limits on the validity scale of these models.

Among the approaches used to introduce LIV on particle physics, two stand out. One is generic, and it is not (necessarily) bounded to a particular model. The other one is based on the spontaneous breaking of the Lorentz symmetry. The former is implemented via a general modification of the single-particle dispersion relation. In contrast, the second mechanism introduces the standard model, a collection of LIV renormalizable operators that preserve energy-momentum and microcausality, among other desired properties of the Standard Model. This extension is named the minimal Lorentz-violating extension of the Standard Model (mSME) [11].

Both mechanisms, the mSME, and the generic LIV, can lead to physics beyond Standard Model. Nevertheless, the generic approach tends to converge quicker and simpler to phenomenology, and it is not necessarily bound to a particular LIV model. Although it can be compatible with the mSME, they usually express their LIV parameters in different ways. In this thesis, we propose to use the derived physics from the mSME as an *ansatz* to build a generic approach with the same physics to contrast the results

with experiments at the highest energetic window, that is, those observing cosmic and gamma rays.

Astrophysical scenarios are an interesting place to test the possible signatures of LIV due to the high energies and very long distances they involve. The effects of LIV are expected to increase with energy for some energetic regime close to the Plank scale. Additionally, the very long distances can lead to a significant LIV effect due to accumulative processes. We have chosen to explore vacuum Cherenkov radiation and photon decay for these purposes for the present study. Both processes are forbidden in the SM physics, but under LIV hypothesis, they are permitted and can lead to extreme scenarios due to their implications on cosmic and gamma-ray propagation. Once our generic approach has been validated, we proceed to explore other processes that are also relevant for cosmic ray propagation, photon decay, and photoproduction processes.

This thesis is organized as follows. In the next chapter, we briefly present both the spontaneous and the generic LIV mechanisms that we use along with this work and a brief on cosmic and gamma-ray physics. In Chapter 3, we present the derived physics for vacuum Cherenkov radiation in two particular models of the mSME and we develop the generic approach for the same phenomena in order to validate our approximation. In Chapter 4, we focus on photon decay, using the LIV generic approach, to show that this phenomenon implies a very restrictive scenario for photon propagation. Consequently, we extract limits for the LIV scale, E_{QG}, to first and second order on the LIV correction, from the direct observation of very high energy photon events H.E.S.S. and HEGRA cosmic gamma-ray telescopes. Besides, a general analysis for photoproduction processes on the cosmic photon background, oriented to evaluate the effects of the generic LIV effects on the determination of the energy thresholds, is presented along Chapter 5. There, we also discuss a secondary energy threshold's appearance, as a signature of LIV, above which photo production becomes forbidden. Finally, the last chapter is dedicated to summarize our results and point to further work.

Chapter 2

Framework

The present work aims to address the phenomenology derived from the LIV hypothesis for cosmic and gamma rays. Therefore, the present chapter presents the necessary framework to address the developments, analyses, and results presented in the following sections. This chapter is divided into two parts; the first one exposes the Coleman and Glashow approximation and particular examples of corrections to the dispersion relation to addressing the generic version of the LIV-modified dispersion relation at any order n, that we use throughout this thesis. We also present the modified Maxwell and Maxwell-Chern-Simon theories as models developed in the literature with which we compare our results in Chapter 3. In the second part, we approach the phenomena of cosmic rays and gamma rays, their propagation, and name some of the observatories dedicated to their study and have measured some of the most energetic photon events relevant to them to the results and conclusions of this thesis.

2.1 Lorentz invariance violation

2.1.1 Basics on Lorentz invariance

To this day, nature has been shown to have four fundamental forces: electromagnetism, weak, strong, and gravity. The first three are very well described by the standard model of particles (SM), while gravity is described by the theory of general relativity (GR). Both, although fundamentally different, have no contradiction in their predictions. Nevertheless, several quantum gravity models seek to unify both fundamental theories in a single one. Among them, we can mention string theory and loop quantum gravity. The resulting new physics may involve new properties, such as new space-time dimensions, scenarios with brane worlds, non-commutative geometries, space-time varying fields or

couplings, and among others, that laws of relativity may not be exact, which may derive in a certain violation of the Lorentz invariance that can effectively manifest itself up to some energetic scale.

The SM is a quantum field theory (QFT) build up on special relativity (SR), whose properties and symmetries are well known. To mention some, it is invariant under the continuous gauge symmetry SU(3)×SU(2)×U(1) and the consecutive application of Charge conjugation, parity transformation, and Time reversal symmetry (CPT). In the SM, some of these symmetries may be broken, explicitly like CP in the electroweak sector and some meson interactions, and spontaneously as in the electroweak model's Higgs mechanism. However, for local interactions of point-like particles in QFT, strong experimental constraints imply that CPT must hold. Theoretically speaking, the conservation of CPT in QFT is a consequence of Lorentz invariance. So, any CPT violation search is also a LIV look. However, not every LIV involves a violation of CPT conservation. An alternate form of CPT violation, which keeps LI arises when non-local interactions are involved in the theory, but we are not concerned about those in here.

On the other hand, GR is a geometric theory where gravity's effects are given by the curvature of space-time and described by the metric tensor, the Riemann Curvature, and Ricci tensors the scalar Curvature. This theory is invariant under diffeomorphisms and is locally Lorentz invariant.

Lorentz invariance (LI) plays a central role in relativity and models that describe the fundamental forces. It is noteworthy that in special relativity, LI holds as a global symmetry, but it is a local symmetry in general relativity.

To illustrate LI implications in the SM and following Ref. [12], let be a scalar, vector, tensor or a spin field, Φ, which transforms globally in some representation D of the Lorentz group SO(1,3), also let be A $\in$ O(3,1) and $D(A)$ some finite-dimensional representation of Lorentz group, then, the action of A on Φ is affected by a unitary operator in Hilbert space, $U(A)$, that satisfies:

$$U(A)^{\dagger}\Phi(x)U(A) = D(A)\Phi(A^{-1}x). \tag{2.1}$$

The Lie Algebra of the Lorentz group, SO(3,1), can be expressed as the complete sum of two angular momenta, $J^{(+)}$ and $J^{(-)}$, such that

$$[J^{(+)}, J^{(-)}] = 0.$$

An irreducible finite-dimensional representation of the group may be labeled by two half integers, j_+ and j_-, and dimension $(2j_+ + 1)(2j_- + 1)$. The ladder operators j_+ and

j_- can take explicit values depending on the field. To specify the field classification see Table 2.1.

$\mathbf{\Phi(x)}$	$(\mathbf{j_+, j_-})$	**Notes**
Scalar	$(0,0)$	
Weyl spinor	$(1/2,0)$ $(0,1/2)$	Depending on its Chirality
4-vector	$(1/2,1/2)$	
Tensor	$(1,1)$	For a traceless and symmetric vector
	$(1,0)\oplus(0,1)$	For an antisymmetric tensor

TABLE 2.1: Field classification and values of (j_+, j_-).

It is well known that Lorentz transformations include rotations and Lorentz boosts, so let be $R(e,\theta)$ a rotation on axis $\vec{e}$ by an angle θ and $B(e,\phi)$ a boost in a direction $\vec{e}$ by rapidity ϕ, then, the effect of D satisfies

$$D(R(e,\theta)) = \exp -i(\vec{J}^{(+)} + \vec{J}^{(-)}) \cdot \vec{e}\,\theta, \tag{2.2}$$

and

$$D(B(e,\phi)) = \exp i(\vec{J}^{(+)} - \vec{J}^{(-)}) \cdot \vec{e}\,\phi. \tag{2.3}$$

Additionally, since CPT invariance is a consequences of LI, let be Ω the anti-unitary CPT operator, then

$$\Omega^{-1}\Phi(x)\Omega = (-1)^{2j_+}\Phi^\dagger(-x). \tag{2.4}$$

Eq. (2.2) implies that every rotationally invariant term $\mathcal{L}'$ in the Lagrangian must lie in a representation form which $j_+ = j_- = j$. So, from elementary angular-momentum theory, m runs from j_- to j_+ and any additional term, as presented in Ref. [12], has to be proportional to

$$\mathcal{L}' \propto \sum_{m=-j}^{j} (-1)^m \Phi_{m,-m}, \tag{2.5}$$

and the expectation value for a state $|\psi\rangle$ boosted in the z-direction by a rapidity ϕ, should be

$$\langle\psi|\, U^\dagger(B(\vec{e}_z\phi))\; \mathcal{L}(0)\; U(B(\vec{e}_z\phi))\; |\psi\rangle \;\propto\; e^2\, \langle\psi|\, \Phi_{j,-j}(0)\; |\psi\rangle \;+ O(e^{(2j-2)\phi}). \tag{2.6}$$

where the fields Φ_{m_+,m_-} form the basis of the irreducible representation and $m_\pm$ are the eigenvalue of $J_z^{(\pm)}$.

Therefore, the rotationally-invariant possibilities are $j = 1, 1/2, 0$, which are a CPT-even tensor, a vector CPT-odd vector and a LI scalar, respectively.

As an example, for a real scalar field, the only possible contribution as a Lorentz invariant needs at least two derivative operators and by renormalizability no more than two scalar fields per term, so

$$\frac{1}{2}\sum_a \partial_\mu \phi^a \partial^\mu \phi^a = \frac{1}{2}\sum_a (\partial_0 \phi^a \partial^0 \phi^a - \partial_i \phi^a \partial^i \phi^a), \tag{2.7}$$

where μ is a Lorentz index, and the sum runs over the scalar fields.

In the momentum space, Eq. (2.7) can lead to the LI dispersion relation for one real scalar field of mass m,

$$E^2 - p^2 = m^2. \tag{2.8}$$

2.1.2 LIV-dispersion relation

2.1.2.1 Quadratic corrections

As presented in the previous section, the allowed form in Eq. (2.7) is a consequence of global LI in the scalar sector ($j = 0$) in QFT. Moreover, the difference $\partial_0 \phi^a \partial^0 \phi^a - \partial_i \phi^a \partial^i \phi^a$ is a Lorentz invariant. Hence, the following term, proposed in Coleman and Glashow work [12], induces LIV in the scalar sector,

$$\frac{1}{2}\sum_{ab} \partial_C \phi^a \epsilon_{a,b} \partial^C \phi^b, \tag{2.9}$$

where the sum runs over the scalar fields, $\epsilon_{a,b}$ is a real symmetric matrix, and $C = \{0, i\}$ indicates either the temporal o spatial derivative.

Once the Lagrangian is established, particle properties of free fields follow from it. As an example and for simplicity, one can look for the analogous of Eq. (2.8), the energy-momentum relation for one real scalar field of mass m. In a Lorentz invariant theory,

$$-iD^{-1} = (p^2 - m^2)A(p^2) \tag{2.10}$$

is the re-normalized propagator for some function A. Now, adding the Lorentz-violating interaction to the theory using some small coefficient ϵ, the change or shifts in the zeroes of D^{-1}, to first order in ϵ, is

$$E^2 - p^2 = m^2 + \epsilon\, \vec{p}^{\,2}. \tag{2.11}$$

Notice that in Eq. (2.11) the correction to the dispersion relation is quadratic.

The generalization to more complicated systems is straightforward. For instance, for spinors ($j = 1/2$), the LIV-induced term takes the form

$$\frac{1}{2}\sum_{a,b} i\epsilon_{ab} u^{a\dagger}\vec{\sigma}\cdot\vec{\partial}u^{b}, \tag{2.12}$$

where ϵ_{ab} is an Hermitian matrix, u^a is a Weyl spinor from a set n(1/2,0) and $u^{a\dagger}$ is its conjugate field, which is a (0,1/2) spinor.

2.1.2.2 Cubic corrections

Another useful example arises from dimension five operators in an effective field theory that would lead to $O(E^3)$ modifications of the dispersion relations. To illustrate this, we follow the model presented in [13]. In this work, the authors adopt the approach where Lorentz symmetry is broken by a background four-vector n^a. The operators satisfy:

1. It is quadratic in the same field.
2. Gauge invariant.
3. Lorentz invariant, but n^a.
4. Not reducible to a total derivative.
5. Not reducible to lower dimension operators by the equations of motion.
6. Have one additional derivative than the usual kinetic term.

Additionally, to ensure that all operators of dimension five can be regarded as small perturbations, they are assumed to be suppressed by a factor of $1/M_{Pl}$, where M_{Pl} is the Plank mass scale.

For the scalar case, the possible term is a CPT-odd contribution:

$$\mathcal{L}^{(5)}_{scalar} = i\frac{\kappa}{M_{Pl}}\bar{\Phi}(n\cdot\partial)^3\Phi, \tag{2.13}$$

where Φ could be a real or a complex scalar field[1].

In the momentum space and in the Lorentz frame where $n^a = (1,0,0,0)$, $n\cdot\partial \approx -iE$, thus, Eq. (2.13) leads to the dispersion relation

$$E^2 \approx |\vec{p}|^2 + m^2 + \frac{\kappa}{M_{Pl}}|\vec{p}|^3, \tag{2.14}$$

[1]However, as the authors point out in [13], the real case is a total derivative and does not change the dispersion relation.

which is a cubic correction to the scalar dispersion relation.

For the vector case, the proposed nontrivial modification of the dispersion relations that fulfill at leading order Maxwell equations in vacuum and Bianchi identities is

$$\mathcal{L}_{\gamma}^{(5)} = \frac{\xi}{M_{Pl}} n^a F_{ad} n \cdot \partial (n_b \tilde{F}^{bd}). \tag{2.15}$$

Once again, in momentum space, for photons traveling along z-axis, $k^a = (E, 0, 0, p)$ and for transverse polarizations along xy-axes, the dispersion relation becomes

$$\left(E^2 - |\vec{p}|^2 \pm \frac{2\xi}{M_{Pl}} p^3 \right) (\epsilon_x \pm i\epsilon_y) = 0, \tag{2.16}$$

where the sign of the cubic term is determined by the chirality of photons.

Finally, for spinor cases, authors in Ref. [13] propose the term

$$\mathcal{L}_f = \frac{1}{M_{Pl}} \bar{\Psi} (\eta_1 \not{n} + \eta_2 \not{n} \gamma_5) (n \cdot \partial)^2 \Psi, \tag{2.17}$$

where both operators are CPT-odd. Now, the dispersion relation takes the form

$$E^2 - |\vec{p}|^2 - m^2 - \frac{2|p|^3}{M_{Pl}} (\eta_1 + \eta_2 \gamma_5) = 0. \tag{2.18}$$

In this effective field theory construction, Eqs. (2.14), (2.16) and (2.18) are cubic corrections to the dispersion relation motivated by dimension five operators that violate LI.

2.1.2.3 n-th corrections

LIV-induced modifications to the dispersion relation are common in literature and astroparticle physics phenomenology, particularly those that modify the photon dispersion relation. For instance, in Ref [14] authors use a series expansion of the form

$$E^2 \approx p^2 \times \left[1 - \sum_{n=1}^{\inf} s_{\pm} \left(\frac{E}{E_{QG}} \right)^n \right], \tag{2.19}$$

where, E_{QG} is the energy scale of Quantum Gravity. At leading order term, the photon propagation speed is

$$v_{ph}(E) = \frac{\partial E}{\partial p} \approx 1 \times \left[1 - s_{\pm} \frac{n+1}{2} \left(\frac{E}{E_{QG}} \right)^n \right]. \tag{2.20}$$

This approximation has been used to claim that due to the energy dependence of $v_{ph}(E)$, two photons of different energies emitted by a distant source at the same time and form

the same location will arrive on Earth with a time delay, Δt, which depends on their energies. This ansatz has set several limits in E_{QG} by the studying of TeV/MeV/GeV emission. For instance, in Ref. [14] bright Gamma-Ray Bursts (GRB) are used.

2.1.3 Generic LIV dispersion relation

A phenomenological generalization of the previous formalisms converges to introducing an additional term in a single particle's dispersion relation. As it has already been said, this generalization is perhaps the most commonly used on phenomenology studies since it offers a clear idea on the derived physics from the LIV hypothesis and it is not necessarily bound to a particular LIV-model [10, 15–24]. We name this generalization **Generic LIV mechanism** since the extra term in the particle relation can be motivated by the introduction of a not explicitly Lorentz invariant term at the free particle Lagrangian as the formalism presented in Sections 2.1.2.1 and 2.1.2.2. The extra term is restricted by a dimensionless coefficient, which we call by convenience ϵ.

To the lowest order, the new dispersion relation for a free particle takes the form:

$$E^2 - p^2 \pm \epsilon A^2 = m^2, \tag{2.21}$$

where $(E, \vec{p})$ stand for the four momenta associated with a given particle of mass m. We use the shorthand notation $p = |\vec{p}|$. A can take the form of E or p; however, for the ultra-relativistic limit where $m \ll \{E, p\}$, any particular choice of A will be equivalent. We will choose the sign of ϵ according to whether we correct energy or momentum, leaving a positive sign for energy. For simplicity, we shall take $A = p$ in most of this thesis, but in Chapter 5, we use $A = E$.

The most general modification to the dispersion relation would instead involve a general function of energy and momentum, such that one could write

$$E^2 - p^2 + \epsilon(A)A^2 = m^2. \tag{2.22}$$

As previous examples in Sections 2.1.2.1-2.1.2.3, we ask that the LIV term can only be relevant at high energies, so ϵ should be small, which guarantees that the physics at low energies remains Lorentz invariant. Thus, we can use a Taylor expansion

$$\epsilon(A)A^2 = \epsilon(0)A^2 + \epsilon'(0)A^{(2+1)} + \frac{\epsilon''(0)}{2!}A^{(2+2)} + \frac{\epsilon'''(0)}{3!}A^{(3+2)} + ... \tag{2.23}$$

However, to study the underlying physics, one can keep one term of order n at once, assuming it as the leading term. On this assumption the dispersion relation becomes

$$E^2 - p^2 \pm \alpha_n A^{n+2} = m^2, \tag{2.24}$$

where $\alpha_n = 1/M^n = 1/(E_{LIV}^{(n)})^n$ defines the energy scale associated to the LIV physics. $\epsilon^{(n)}$ derivatives are assumed over a vactor $1/M^n$. E_{LIV} is commonly associated with the energy scale of Quantum Gravity, E_{QG}, which is expected to be close to the Planck scale, $E_{Pl} \sim 10^{19} GeV$. In the literature, one can find upper limits to $E_{QG}^{(n)}$ obtained by different techniques, even beyond the Planck scale [14, 25–33]. A small list of the current limits for $E_{QG}^{(1,2)}$ is presented in Table 2.2.

Notice that the dispersion relation in Eq. (2.11) corresponds to the special case in Eq. (2.24) for $n = 0$. Similarly, Eqs. (2.14), (2.16) and (2.18) stand for $n = 1$, and Eq. (2.19) for any n. That is, Eq. (2.24) can be derived from a particular LIV model but it is not necessarily bounded to them. Additional examples can be found in [10, 15–23].

Source	**Experiment**	$\mathbf{E_{QG}^{(1)}}$	$\mathbf{E_{QG}^{(2)}}$	**Dist.**	**Analysis**
GRB 090510	Fermi- LAT	9.1×10^{19}GeV	1.3×10^{11}GeV	$z = 0.903$	combined methods
PKS $2155 - 304$	HESS	2.1×10^{18}GeV	6.4×10^{10}GeV	$z = 0.116$	likelihood fit
PG $1553+$ 113	HESS, Fermi- LAT	4.3×10^{17}GeV	2.1×10^{10}GeV	$z \approx 0.49$	combined analysis
Crab	Veritas	1.7×10^{17}GeV	7×10^{9}GeV	2.2 kpc	Δt=100μs,[2] E_{max}=120GeV

TABLE 2.2: Short list of lower limits for $E_{QG}^{(1,2)}$ [26].

2.1.4 mSME

In finding a theoretical description that includes Lorentz or CPT violation, a series of publications dating from 1989 from Kostelecky et al. [34] have presented the developments of a theoretical framework to describe Lorentz and CPT violation. They stand that the latter is compatible with the experimental constraints and the established quantum field theory.

The theory suggests that apparent breaking of CPT and Lorentz symmetry might be observable in existing or feasible experiments. It leads to a general phenomenology for CPT and Lorentz violation at the level of SM of particle physics and Einstein's theory of

[2] For more details on Δt and E_{max} reader could refer to section 2.1.2.3

gravity, General Relativity. That is, Kostelecky et al. constructed a generalization of the usual SM and GR models, such that it has the conventional and desirable properties of the SM, but that allows violation of Lorentz and CPT symmetry, and they have called it the standard model extension (SME). This proposes the inclusion of all the contributions to the SM that violate Lorentz symmetry by spontaneous symmetry breaking (SSB) [1, 2][3], i.e., all observer-scalar terms that are products of SM and gravitational fields which are not Lorentz invariant and generically require couplings that explicitly carry Lorentz indices.

The minimum set of such operators that maintain gauge invariance and power-counting renormalizability conform to the so-called mSME [11]. A useful classification of these new terms arises by separating out the sectors of the SM, such as the $\mathcal{L}_{lepton}$ or $\mathcal{L}_{gauge}$, for lepton or gauge sectors, respectively. Additionally, such operators can be classified into those that break CPT symmetry and those that do not. They are named *CPT-odd* and *CPT-even* respectively. For a complete list of the operators in the mSME see Appendix A.

For this work, we have chosen the photon sector with the following additional contributions to the standard Lagrangian density,

$$\mathcal{L}_{photon}^{CPT-even} = -\frac{1}{4}(k_F)_{\rho\lambda\mu\nu}F^{\rho\lambda}F^{\mu\nu}, \tag{2.25}$$

and

$$\mathcal{L}_{photon}^{CPT-odd} = \frac{1}{2}(k_{AF})^{\rho}\epsilon_{\rho\lambda\mu\nu}A^{\lambda}F^{\mu\nu}, \tag{2.26}$$

with the gauge field A_μ and the field strength tensor $F_{\mu\nu} = \partial_\mu A_\nu - \partial_\nu A_\mu$. In above $\epsilon_{\mu\nu\rho\lambda}$ is the antisymmetric Levi-Civita symbol. The coefficients k_F and k_{AF} in Eqs. (2.25) and (2.26) are the ones that break particle Lorentz Invariance. To fulfill power-counting renormalizability, k_F should be dimensionless and k_{AF} should has a mass dimension one. On the analysis regarding this sector, it is usual not to assume the simultaneous presence of LIV corrections for fermions, and we are going to do so in our study along the following sections.

The *CPT-even* term can be studied separately as in the so-called modified Maxwell theory (modM [35]),

$$\mathcal{L}_{modM} = -\frac{1}{4}F_{\mu\nu}F^{\mu\nu} - \frac{1}{4}\kappa^{\mu\nu}{}_{\rho\lambda}F_{\mu\nu}F^{\rho\lambda}. \tag{2.27}$$

$\kappa^{\mu\nu}{}_{\rho\lambda}$ is a dimensionless fourth rank tensor, with 256 components, but it is usually assumed to have vanishing double trace, $\kappa^{\mu\nu}{}_{\mu\nu} = 0$, since any trace component can be

[3] The use of spontaneous breaking of Lorentz symmetry can be traced back by Y. Nambu in 1968 [1]. A fine review of state of the art can be found in [2].

redefined in the kinetic photon term. It is also demanded to obey the same symmetries which hold for the Riemann curvature tensor,

$$\kappa_{\mu\nu\rho\lambda} = -\kappa_{\nu\mu\rho\lambda} = \kappa_{\nu\mu\lambda\rho}, \quad \kappa_{\mu\nu\rho\lambda} = \kappa_{\rho\lambda\mu\nu}, \tag{2.28}$$

such that only 19 independent components remain [36]. However, the following *ansatz*, used in Ref. [11, 35], reduces the number of independent parameters from 19 to 1.

$$\kappa^{\mu\nu\rho\lambda} = \frac{1}{2}(\eta^{\mu\rho}\tilde{\kappa}^{\nu\lambda} - \eta^{\mu\lambda}\tilde{\kappa}^{\nu\rho} + \eta^{\nu\lambda}\tilde{\kappa}^{\mu\rho} - \eta^{\nu\rho}\tilde{\kappa}^{\mu\lambda}), \tag{2.29}$$

and

$$\tilde{\kappa}^{\mu\nu} = \frac{3}{2}\tilde{\kappa}_{tr}\ \mathrm{diag}(1, 1/3, 1/3, 1/3), \tag{2.30}$$

where Eq. (2.29) restricts the theory to the nonbirefringent sector, and Eq. (2.30) does it to the isotropic sector.

On the other hand, the CPT-*odd* term is studied in the spacelike Maxwell-Chern-Simons theory (MCS [37]), with the following Lagrangian density,

$$\mathcal{L}_{MCS} = -\frac{1}{4}F_{\mu\nu}F^{\mu\nu} + \frac{1}{4}M_{CS}\epsilon_{\mu\nu\rho\lambda}\xi^{\mu}A^{\nu}F^{\rho\lambda}, \tag{2.31}$$

where $M_{CS} \sim 1/L_0 \approx 2 \times 10^{-33}$ eV is the Chern-Simons mass scale [37, 38] and $\xi_\mu = (0, 0, 0, 1)$ is the fixed space-like normalized Chern-Simons vector. Notice that this model is not rotationally invariant, so energy-momentum will be conserved but angular momentum shall not.

It is noteworthy that in Eqs. (2.24), (2.25) and (2.26) the involved coefficients are not necessarily the same and so, numerically,

$$k_F \neq k_{AF} \neq \alpha_n, \tag{2.32}$$

despite that, all of them parametrize the LIV hypothesis. Hence, the values and limits that can be derived for them shall be different too. Therefore, for comparison proposes with the LIV generic approach, we will use the limit values given in the literature for the involved parameters of modM and MCS models. For a complete list of the current constraints and limits of the SME see [39].

2.2 A Brief on Cosmic and Gamma Ray Physics

2.2.1 Cosmic Rays

Cosmic rays (CR) are the most energetic phenomena known so far, reaching energies of some decades of EeV [40]. Among the many particulars their study and understanding reveal, they also provide an energy window to test fundamental physics. Such is the case of the search for signatures of LIV.

Today we know that there are cosmic rays from our Solar System, our Galaxy, and beyond. However, the origin of the most energetic particles remains an open question. Most of the cosmic rays are charged particles and atomic nuclei. They commonly have a lifetime of the order of 10^6 years or more. Cosmic rays generated and accelerated at an astrophysical source can be protons, electrons, helium nuclei, oxygen, iron, and other basic elements made in the stars. In their interstellar and intergalactic propagation, they interact with the interstellar media and interstellar magnetic field, generating a secondary contribution of boron, lithium, beryllium, and another atomic nucleus. Cosmic rays that arrive at the top of the Earth's atmosphere are named primary CR. Secondary CRs are the result of interactions among primary CR and atomic nuclei in the atmosphere. These interactions usually take place at an altitude between 10 to 15 kilometers from the ground. The primary energy is divided among the secondaries that repeat the process. As a result, a particle shower is created.

The passage of CR through the atmosphere excites nitrogen molecules from the air and produces ultraviolet (UV) light, seen by fluorescence detectors. At ground level, secondaries can be detected in arrays of particle detectors, such as scintillation counters or water tanks. At sea level, the most common secondary cosmic rays are muons. These, on average, arrive at sea level with an energy of the order of four GeV with a rate of a muon per cm^2 per minute. Only muons, neutrinos, and antineutrinos can penetrate and spread significantly through the Earth's crust.

2.2.1.1 Cosmic ray energy spectrum

The cosmic ray energy spectrum varies continuously from energies of the order of 10 MeV to extraordinarily high energies of the order of 10^{20} or 10^{21} eV, as is depicted in Fig. 2.1. It has been estimated that although 10^{13} cosmic rays from outer space hit the top of the atmosphere per second, the total energy received by the Earth from them is comparable to that associated with the light from the stars at sea level.

The intensity of cosmic rays changes with latitude: in the North and South poles' direction, it is greater than that at the equator (approximately 10 percent). This effect is due to the Earth's magnetic field, in those regions, which deflects cosmic charged particles at low energies, which are the most abundant in the CR flux.

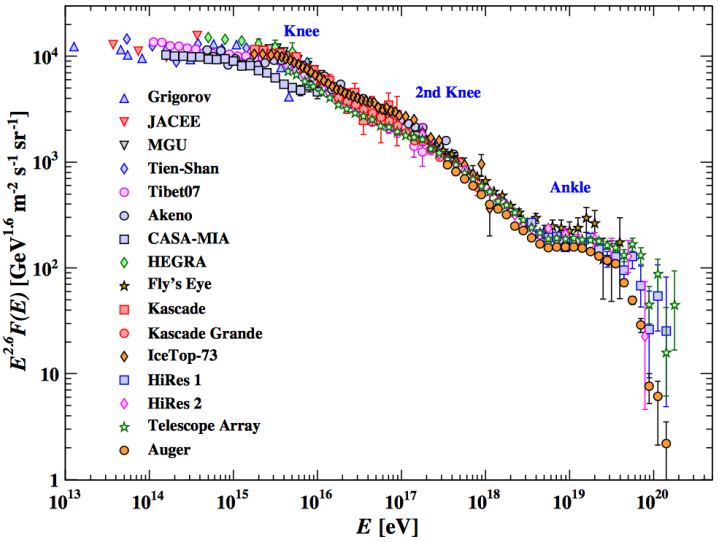

FIGURE 2.1: The cosmic ray energy spectrum. It covers at least 11 orders of magnitude in the energy and close to 32 orders in the flux. Measurements by several Observatories are compatible with the shape of the spectrum. [41]

The cosmic ray energy spectrum has an approximate power law behaviour, given by

$$\frac{dN}{dE} \propto E^{-\alpha}, \tag{2.33}$$

where α is the spectral index, $\alpha \approx 2.7$. It has been shown that the all-particle spectrum shows two main features, which are called the *knee* and *ankle* at $2 - 5 \times 10^{15}$ eV and $2 - 8 \times 10^{18}$ eV, respectively. At the *knee* the spectrum steepens to $\alpha \approx 3.0$, while the ankle is characterized by a flattening of the spectrum by where the spectral index backs to $\alpha \approx 2.7$ [42]. Additionally, somewhere in the energy range from 10^{16}eV to a few 10^{18} eV, the end of cosmic rays of galactic origin is expected. Thus, *knee-like* features could be distributed inside this energy interval. Experiments as KASKADE-Grande have been studying the possible presence of these individual features in the all-particle energy spectrum, called de 2nd knee [42–45]. At energies above the *ankle*, in the UHECR regime, $\alpha = 2.8$ and is followed by a sharp ending of the spectrum [40], where the cosmic ray flux is about one CR with the energy of 10^{20}eV per km^2 per century. This suppression is commonly associated with the Greisen-Zatsepin-Kuzmin (GZK) cutoff [40, 46, 47]. This comes about because hadronic particles, such as protons, interact with the cosmic microwave background (CMB) through the following reactions:

$$\gamma + p \rightarrow \Delta^+ \rightarrow p + \pi^0, \tag{2.34}$$

$$\gamma + p \rightarrow \Delta^{+} \rightarrow n + \pi^{+}. \tag{2.35}$$

Using special relativity, the threshold energy of the pion photoproduction in a Lorentz invariance regime is

$$E_{p_{th}} \approx \frac{m_\pi(2m_p + m_\pi)}{4\omega_b}, \sim 1 \times 10^{20} eV. \tag{2.36}$$

where $\omega_b \approx 2.7$ K $\times$ (11 604.5 eV/K)$^{-1} \approx 2.3 \times 10^{-4}$eV is the CMB photon energy; $m_p \approx 938.27$ MeV and $m_\pi \approx 134.98$ MeV, are the rest masses of the proton and neutral pion, respectively, and $E_{p_{th}}$ is the threshold energy of the incident proton in the laboratory system for pion photoproduction.

The effective cross section for the processes in reactions (2.34-2.35) and close to the threshold is $\sigma = 2 \times 10^{-28}$ cm^2, while the total microwave density is $\rho = 400$ cm^{-3}. Thus, the mean free path for the above collision is about $\lambda = \frac{1}{\rho\sigma} = 10^{25}$ cm. So, cosmic rays with energies above 10^{20} eV that travel distances greater than 10^{25}cm will be attenuated to energies lower than the threshold $E_{p_{th}}$.

Strong consequences are derived from this phenomenon, such that the origin of the UHECR must be from cosmologically close sources. The energy calculated in Eq. (2.36) predicts the so-called GZK horizon, corresponding to ~ 50 Mpc for protons, the maximum distance from which the UHECR-protons would come. LI plays a central role in this prediction. In Chapter 6, we present scenarios where the introduction of LIV could drastically change this conclusion.

The origin, production, acceleration, and propagation mechanisms of UHECR and beyond are still unknown. The mass composition of UHECR is expected to reveal valuable information on the origin and acceleration mechanisms [48]. The existence of a light component in the CR flux at the highest energies is crucial for astronomy with charged particles to be feasible [49]. Moreover, UHECR observatories as the Pierre Auger Observatory (PAO) and Telescope Array have found that the mass composition at the end of the CR spectrum is mixed and varies between protons and iron nuclei [50]. In Chap. 3, we show that LIV processes as vacuum Cherenkov radiation may be compatible with a mixed mass composition. However, a detailed calculation is needed to understand better the extension of ultra high energy cosmic rays' effect.

There are generally two types of scenarios to explain the CR origin, the acceleration scenarios, commonly named *bottom-up*, and the decay scenarios, called *top-down* [51]. In the first ones, it is assumed that all highly energetic charged particles are accelerated by interaction with magnetic fields in a shock front in relativistic plasmas (second-order

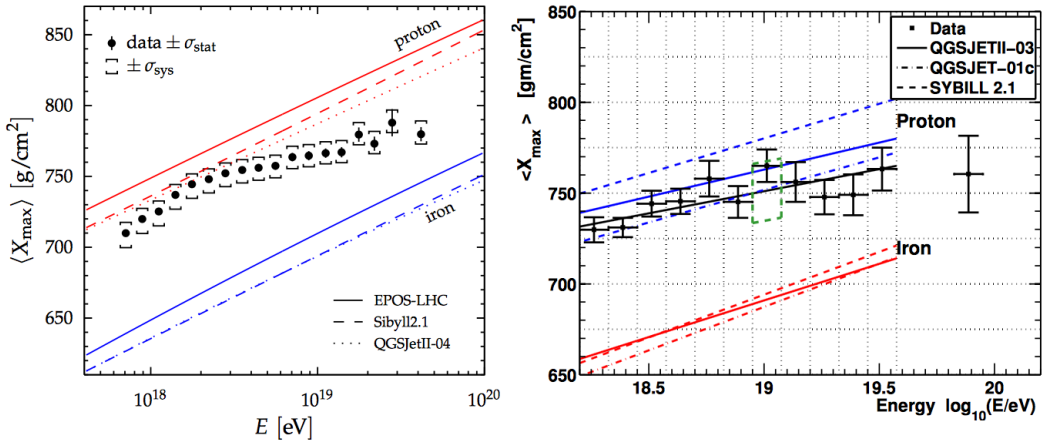

FIGURE 2.2: The $\langle X_{max} \rangle$, measured by Pierre Auger and Telescope Array Collaborations, show that the mass composition at the most energetic window varies between protons and iron nuclei. [50]

Fermi acceleration, proposed by Fermi in 1949 [52]); this idea can reproduce the power-law spectrum. However, there is still uncertainty in the origin and acceleration of the highest energy cosmic rays [48, 53].

In the second scenario, the decay type, UHECR are predicted due to the decay of high-energy particles. For instance, some exotic particles are suggested by theories beyond the SM [54, 55]. Under this scenario, the neutrino and gamma-ray fluxes are derived through the decay of π-meson produced in the hadronization of quarks. Their observation is a discriminator between scenarios [56, 57].

Both models, the acceleration and decay type, have been heavily restricted by the measurements made by current Telescopes and Observatories at the very high and ultra-high energetic window. However, the search for UHE-photons [58] has highly restricted some *top-down* models.

2.2.2 Gamma Rays

The energy spectrum of cosmic rays measured at Earth exhibits a power-law dependence over a wide range of energy, as it was mentioned in section 2.2.1.1. Starting at a few GeV it continues to energies of at least 10^{20} eV. Up to energies $\sim 10^{17} - 10^{18}$ eV, cosmic rays are believed to be of Galactic origin and accelerated in *bottom up* mechanisms, for instance, shell-type supernova remnants (SNR) and pulsars. They are believed to be of extragalactic sources for higher energies, like active galaxies or gamma-ray bursts (GRB).

However, the experimental confirmation of a particular source of Galactic cosmic rays is difficult due to the propagation effects of charged particles in the interstellar medium. The most promising way of proving the existence of high-energy particles is the detection of very high energy (VHE) gamma rays (E > 100 GeV), produced in interactions of cosmic rays with the ambient matter close to their acceleration site.

Hence, gamma-ray observations give a direct view of the most extreme environments of the universe. They play the leading role to study astronomical particle accelerators and help to understand the propagation of cosmic rays through the Milky Way. Gamma-rays are also used to perform dark matter searches, gamma-ray, neutrino astronomy, and fundamental physics studies, like LIV-searches. In this thesis, some of the most energetic gamma-ray observations are used to set constraints to Lorentz invariance violation on cosmic and gamma rays. Therefore, in the following sections, we present some of the telescopes' observations dedicated to looking at the sky at very high energies.

2.2.2.1 HESS

The High Energy Stereoscopic System (HESS) is an array of five imaging atmospheric Cherenkov telescopes located in the Khomas Highland in Namibia, at the height of 1800 m above sea level, which observes the gamma-ray sky in the energy range from GeV to TeV. The Telescope name pays homage to Victor Hess, who received the Nobel Prize in Physics in 1936 by discovering cosmic radiation.

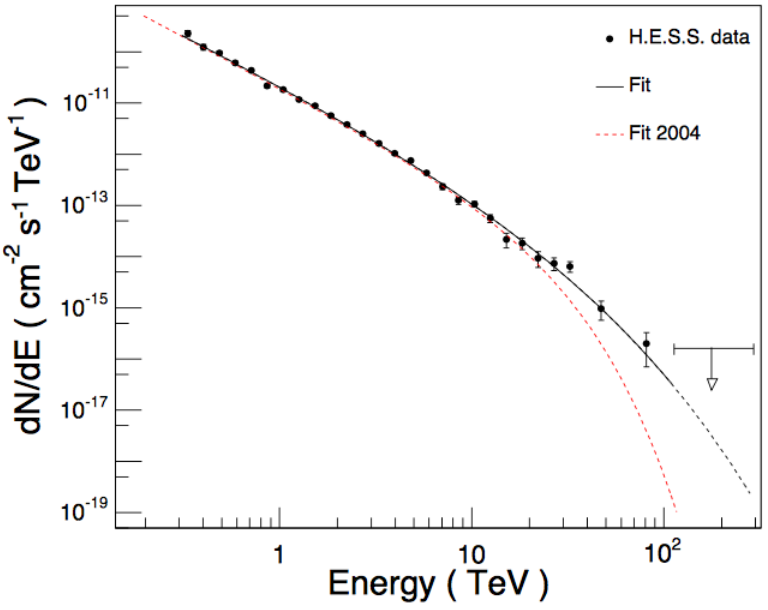

FIGURE 2.3: Combined H.E.S.S. gamma-ray spectrum from data of 2003, 2004 and 2005 of the supernova remnant (SNR) RX J1713.7-3946 [59].

In Fig. 2.3, the combined data from 2003 to 2005 are shown; they correspond to observations of the supernova remnant (SNR) RX J1713.7-3946 [59, 60]. The reported cumulative significance above 30 TeV is 4.8 σ. The bin values close to 30 TeV in Fig. 2.3 are presented in Tab. 2.3. For energies between 113 and 294 TeV, they obtained an upper limit on the gamma-ray flux of 1.6×10^{-16}cm^{-2} s^{-1}. At zenith, the energy threshold was about 100 GeV, and for point sources, HESS achieved an energy resolution of 15% [59]. The measured gamma-ray energies imply that the efficient acceleration of primary particles to energies exceeding 100 TeV is taking place in the shell of the SNR RX J1713.7-3946.

# Bin	**E (TeV)**	**Flux (cm^2 s^{-1})**	σ	**Range (TeV)**
24	26.85	$(8.82 \pm 2.46) \times 10^{-15}$	3.6	24.50 to 29.66
25	32.50	$(7.7 \pm 1.79) \times 10^{-15}$	4.3	29.66 to 35.91

TABLE 2.3: Bins 24 and 25 of the 28 bins in Fig. 2.3. Values are taken from Ref. [59]. The statistical significance σ was calculated following Li & Ma analysis [61] by HESS Collaboration.

2.2.2.2 HEGRA

The High Energy Gamma Ray Astronomy (HEGRA) experiment was located on La Palma (Canary Islands) at the height of 2200 m above sea level. HEGRA consisted of several detectors made to measure the light from Extensive Air Showers produced by CR in the energetic window from 1 TeV to 10^4 TeV. HEGRA Telescope took data from 1987 to 2002.

Fig. 2.4 shows the Crab supernova remnant spectrum, measured by the five imaging air Cherenkov telescopes that were part of HEGRA. Nonthermal processes predominantly produce the Crab Nebula emission, synchrotron, and inverse Compton radiation, which form a continuum emission covering the range from radio to VHE gamma-rays [62]. The Crab has been used for the past 25 years as a reference source in TeV astronomy.

The reported differential upper limit flux on pulsed emission at $\langle E \rangle = 56.569$ TeV, in an energy range 32 to 100 TeV, is about 0.2×10^{-16}cm^{-2} s^{-1}. The bin values for close to 56 TeV in Fig. 2.4 are presented in Tab. 2.4. The relative HEGRA energy resolution, σ_E/E, typically reaches values below 10% for energies above the threshold and moderately increases to 15% at threshold energies.

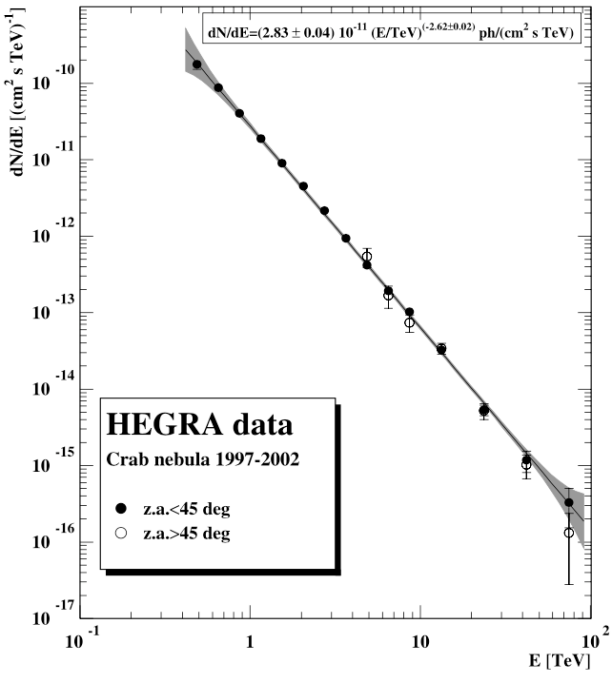

FIGURE 2.4: Differential gamma-ray energy spectrum for the Crab Nebula and Pulsars, reported by HEGRA Collaboration in an energetic window from 0.5 to 100 TeV. The shaded region indicates the range of systematic errors. [62]

# Bin	E (TeV)	Flux (cm^2 s^{-1})	σ	Range (TeV)
14	42.170	$(1.10 \pm 0.25) \times 10^{-15}$	5.7	31.622 to 56.234
15	74.989	$(2.05 \pm 1.01) \times 10^{-16}$	2.7	56.234 to 100.000

TABLE 2.4: Bins 14 and 15 of the 15 bins in Fig. 2.4. Values are taken from Ref. [62]. The statistical significance σ was calculated following Li & Ma analysis [61] by HEGRA Collaboration.

2.2.2.3 HAWC

The High Altitude Water Cherenkov (HAWC) observatory is a new instrument sensitive to multi-TeV hadron and gamma-ray air showers, operating at a latitude of +19°N and an altitude of 4,100 meters in the Sierra Negra, Mexico. HAWC consists of 300 Water Cherenkov Detectors that densely cover an area of 22,000 m^2 and was completed in early 2015.

HAWC has been used to observe the Crab Nebula at high significance across nearly the full spectrum of energies from 100 GeV to 100 TeV. Fig. 2.5 shows recent results of the Crab photon energy spectrum measured with HAWC [63]. They are from a time-integrated analysis of the Crab using 507 live days of data from November 2014 to June 2016. The systematic errors in HAWC measurements are estimated to be ±50% in the photon flux between 1 and 37 TeV. However, confirmation of the Crab flux establishes the HAWC instrument's sensitivity for surveys of the sky. HAWC will exceed the sensitivity

of current-generation observatories and will open a new view of the sky at the TeV energy scale that will bring new opportunities to search for new physics signatures.

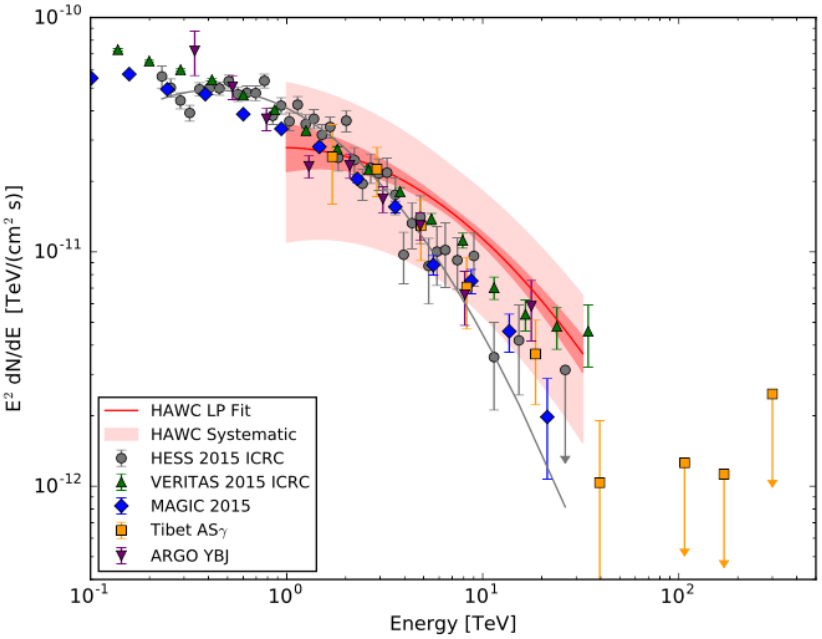

FIGURE 2.5: The crab photon energy spectrum was measured with HAWC and compared to other measurements using other instruments. The red band showed for HAWC is the ensemble of fluxes allowed at 1σ, and the best fit is indicated with a dark red line. The light red band indicates the systematic of the HAWC flux. [63]

The potential to observe signatures of Lorentz invariance violation with HAWC has been explored in Ref. [26]. The estimated potential of HAWC to set limits to E_{QG} in hypothetical scenarios of GRB and pulsars observations is presented. The potential limits are shown in Tab. 2.5.

Source	**Experiment**	$\mathbf{E^{(1)}_{QG}}$	$\mathbf{E^{(2)}_{QG}}$	**Dist.**	**Analysis**
GRB	HAWC	10^{17} GeV	9×10^{9} GeV	2 kpc	Δt=1ms, E_{max}=500GeV
Pulsar	HAWC	$4. \times 10^{19}$ GeV	1.1×10^{11} GeV	$z = 1$	Δt=1s, [4] E_{max}=100GeV

TABLE 2.5: Potential limits for $E^{(1,2)}_{QG}$ from the observation of a GRB and pulsars with HAWC [26].

However, different analyses can produce more stringent limits, like the one proposed in this thesis in Chapter 4.

[4] For more details on Δt and E_{max}, reader could refer to section 2.1.2.3

Chapter 3

Vacuum Cherenkov Radiation

In this Chapter, we develop a generic approximation for the vacuum Cherenkov radiation (VCR) process and compare it with the results obtained for the rates obtained by isotropic modifications of the CPT-even and CPT-odd modified photon theory, modified Maxwell theory (modM) and Maxwell-Chern-Simons (MCS) theory.

When electrically charged and massive particles ruled by a Lorentz invariant physics are added to the LIV models presented in section 2.1.4, the new terms allow photon emission in LIV-vacuum to happen without an external electromagnetic field; this process is commonly called vacuum Cherenkov radiation (See for instance [12, 23, 35, 37, 64, 65]). In a LI theory, Cherenkov radiation happens when a charged particle moves faster than the phase velocity of light in a medium, then, molecules in the medium are polarized through the charged particle path, and they radiate coherently. Similarly, in vacuum Cherenkov radiation, the LIV-vacuum acts as an optical medium with a nontrivial refractive index; hence, particles with energy above a certain energy threshold are allowed to radiate spontaneously.

To further proceed with our analysis for the generic implementation of LIV and compare the modM and MCS models' outcomes, we restrict our discussion to spin 1/2 particles. However, in a general scenario, the following derived physics is spin-dependent, although either particle with spin 0 or 1/2 is allowed to emit photons.

In this Chapter, we summarize the results for the models presented in subsection 2.1.4, then we develop the rate for VCR in the LIVgen1 approximation, and we compare our results to validate our proposal. In the last section, we present a derived scenario for UHECR.

3.1 Emission Rates

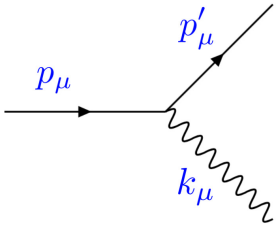

FIGURE 3.1: The Feynman diagram of the spontaneous photon emission (or vacuum Cherenkov radiation).

The process of interest, $l_p \to l_{p'}\ \gamma_k$, is depicted in Fig. 3.1, where the vacuum Cherenkov radiation may correspond in general to leptons, protons and heavy nuclei. The subscript denotes the momentum notation. Hereafter, $(\omega, \mathbf{k})$ stands for the photon four momenta components. Also, $(E, \mathbf{p})$ represents the initial four-momentum of the spin 1/2 charged particle involved in the process, while $(E', \mathbf{p}')$ is for the final four-momentum of the fermion.

3.1.1 Emission rates from modM and MCS theories

The dispersion relations for a single photon in the modified Maxwell theory (modM) and Maxwell Chern-Simons model (MCS) from Refs. [35, 37], presented in section 2.1.4, follow the expressions

$$\omega_{modM}(\mathbf{k}) = \sqrt{\frac{1-\widetilde{\kappa}_{tr}}{1+\widetilde{\kappa}_{tr}}}\ k, \quad k = |\mathbf{k}|, \tag{3.1}$$

$$\omega_{MCS\ \pm}(\mathbf{k})^2 = k^2 \pm M_{CS}\sqrt{k^2\cos^2\phi + \frac{M_{CS}^2}{4}} + \frac{M_{CS}^2}{2}, \tag{3.2}$$

where $\tilde{\kappa}_{tr}$ is the restricted coefficient from Eq. (2.30), for more details please refer to Appendix A. In the MCS expression, ϕ is the angle between the wave vector $\mathbf{k}$ and the space component of the Chern-Simons vector, ξ. $M_{CS} \sim 1/L_0 \approx 2 \times 10^{-33} eV$ is the Chern-Simons mass scale [37, 38]. The subscript $\pm$ denotes two polarization modes.

The reported emission rates for these models are

$$\begin{aligned}\Gamma_{modM} =& \frac{\frac{e^2}{4\pi}}{3\tilde{\kappa}_{tr}^2\sqrt{1-\widetilde{\kappa}_{tr}^2}}\frac{1}{E}\left(\sqrt{\frac{1-\widetilde{\kappa}_{tr}}{1+\widetilde{\kappa}_{tr}}}\frac{E}{\sqrt{E^2-m^2}} - 1\right) \\ &\times\left[\sqrt{\frac{1-\widetilde{\kappa}_{tr}}{1+\widetilde{\kappa}_{tr}}}(3\widetilde{\kappa}_{tr}^2 + 5\widetilde{\kappa}_{tr} + 2)E\sqrt{E^2-m^2}\right. \\ &\left. - (3\tilde{\kappa}_{tr}^2 + 3\tilde{\kappa}_{tr} + 2)E^2 + (3\tilde{\kappa}_{tr}^2 + 4\tilde{\kappa}_{tr} + 1)m^2\right],\end{aligned} \tag{3.3}$$

and

$$\Gamma_{MSC} = \frac{\frac{e^2}{4\pi} M_{CS}}{16E((\mathbf{p}\cdot\xi)^2+m^2)^{1/2}} \Bigg\{ \Big[4\Big(m^2 + 2(\mathbf{p}\cdot\xi)^2 \Big) - M_{CS}^2 \Big] \times arcsinh\left(\frac{2k_{max}}{M_{CS}}\right) + 2(2|\mathbf{p}\cdot\xi| - k_{max})M_{CS} - 4(|\mathbf{p}\cdot\xi| - k_{max})\sqrt{M_{CS}^2 + 4k_{max}^2} - 8m^2\frac{k_{max}}{M_{CS}} \Bigg\}, \tag{3.4}$$

where

$$k_{max} = \frac{2M_{CS}|\mathbf{p}\cdot\xi|(M_{CS} + 2\sqrt{(\mathbf{p}\cdot\xi)^2+m^2})}{M_{CS}^2 + 4m^2 + 4M_{CS}\sqrt{(\mathbf{p}\cdot\xi)^2+m^2}}, \tag{3.5}$$

is the maximum magnitude for the photon momentum component for MCS emission rate.

3.1.2 LIVgen1 emission rate

In this section, we elaborate on the corresponding analysis for the LIV-generic case. There is no clear path to derive the emission rate from the LIV generic approach. However, following the generalities from the two previous models, we can proceed to construct it.

From Eq. (2.24), let be

$$\omega^2 = k^2(1 + \alpha_n k^n), \tag{3.6}$$

the generalized dispersion relation for photons, where α_n is the LIV coefficient of order n. We also neglect, as in previous models, any LIV effect in the corresponding fermion dispersion relations. Then, we develop a generic correction to the emission rate from the standard LI theory, given by

$$d\Gamma = \frac{s}{2}\frac{1}{E(p)}|\mathcal{M}|^2 \frac{d^3p'}{(2\pi)^3 2E'(p')} \frac{d^3k}{(2\pi)^3 2\omega(k,n,\alpha_n)} \times (2\pi)^4\delta^{(4)}(p - p' - k)\ \Theta(k), \tag{3.7}$$

where we have inserted a Heaviside function, $\Theta(k)$, to preserve only physical solutions for the emitted photon momentum. Furthermore, from LI theory, $s = \frac{1}{j!}$ expresses a statistical factor, where j counts one per each group of identical particles in the final stage of the process; and $|\mathcal{M}|^2$ is the squared amplitude probability of the process, computed from the standard QED rules but making use of the correction in the photon four-momenta. With such considerations, we can express the square probability amplitude

as

$$\frac{1}{2}\sum_{spin}|M|^2 = (\not{p}-\not{k}+m)(e^2\gamma^\mu\gamma^\nu)(\not{p}+m)\epsilon_\mu\bar{\epsilon}_\nu$$
$$= 2\sum_{spin}(p^\mu p^\nu - k^\mu p^\nu - p^\nu p^\mu + k^\nu p^\mu + p^\alpha p_\alpha g^{\mu\nu} - k^\alpha k_\alpha g^{\mu\nu} + m^2 g^{\mu\nu})\epsilon_\mu\bar{\epsilon}_\nu \ , \tag{3.8}$$

where Minkowski metric $g^{\mu\nu} = \eta^{\mu\nu}$ and Dirac gamma matrices standard properties under a Lorentz invariant theory are assumed. Since the correction is taken at first LIV order correction, any term $\geq \alpha_n^2$ is negligible, and the Ward identity is preserved.

From Eq. (3.6), $S_\gamma = k^\alpha k_\alpha = \alpha_n k^{n+2}$, and assuming the charged particle dispersion relation to be Lorentz conserving along the process, we note that

$$S_p = S_{p'} = (p-k)^\alpha(p-k)_\alpha = S_p + S_\gamma - 2k^\alpha p_\alpha, \tag{3.9}$$

then

$$2k^\alpha p_\alpha = S_\gamma = \alpha_n k^{n+2}, \tag{3.10}$$

where we have dropped out the particle index on the photon LIV parameter. Hence, Eq. (3.8) becomes:

$$\frac{1}{2}\sum_{spin}|M|^2 = e^2|4m_a^2 - \alpha_n k^{n+2}|. \tag{3.11}$$

The absolute value is taken to ensure physical congruence due to the limits and the generality in the sign of α_n [66]. The delta function in Eq. (3.7) encodes the conservation of energy-momentum in the system. Using Eq. (3.6) and keeping only first order in LIV α_n terms, we made the integration over $\mathbf{p}'$ in Eq. (3.7) and write the remaining delta function as

$$\delta^{(0)}(g(p,k,m,n,\alpha,\theta)) = \quad \delta^{(0)}(\sqrt{p^2+m^2} - \sqrt{(\mathbf{p}-\mathbf{k})^2+m^2} - k\sqrt{1+\alpha_n k^n}), \tag{3.12}$$

where θ is the emission angle and g is a polynomial function of order n in k. To solve the integration in k without the rest frame, that is, only in the observer frame, we use the following well known property of the delta function,

$$\delta(g(x)) = \sum_i \frac{\delta(x-x_i)}{|g'(x_i)|}, \tag{3.13}$$

where x_i are the $g(k_i)$ roots, that we can found from the following expression,

$$\left(p^2\cos^2\theta - (p^2+m^2)\right)k - (p^2+m^2)\alpha_n k^{n+1} + p\ \cos\theta\ \alpha_n k^{n+2} = 0. \tag{3.14}$$

Each solution of Eq. (3.14) implies that the process will satisfy energy-momentum conservation. Note that if $\alpha_n = 0$ then $k = 0$, since $p\cos\theta \neq \sqrt{p^2+m^2}$, and consequently, the process is prohibited for LI scenarios. In other words, the photon emission process in vacuum, or vacuum Cherenkov radiation, is permitted as far as α_n is present.

For $n = 0$, we found that Eq. (3.14) has one solution,

$$k_0^{(n=0)} = \frac{1}{p\cos\theta}\left[E^2(\alpha_0+1) - p^2\cos^2\theta\right]. \tag{3.15}$$

However, for $n = 1$, we found that Eq. (3.14) has three different solutions. That is, in the generic LIV scenario, with $n = 1$, energy and momentum are preserved in at least three different situations, the first one given by the standard case where

$$k_0^{(n=1)} = 0; \tag{3.16}$$

and the second and third ones when

$$k_\pm^{(n=1)} = \frac{1}{2p\cos\theta}\left(E^2 \pm \sqrt{E^4 + \frac{4p\cos\theta}{\alpha_1}(E^2 - p^2\cos^2\theta)}\right). \tag{3.17}$$

In what follows, we only use the mode k_+ for the case $n = 1$, since k_0 means that there is none emission and k_- will be ruled out by the Heaviside function in Eq. (3.7); moreover, it is nonphysical since $k_- < 0$.

Finally, one can use the expressions in Eqs. (3.6), (3.11) and that for k_+ in Eq. (3.17), to perform the integral over k. Hence, the emission rate from the LIV generic approach at first order in α_n (LIVgen1) will be expressed as,

$$\begin{aligned}\Gamma_{a\to a\gamma}^{(n=1)} =& \frac{e^2}{4\pi}\frac{1}{4E}\int_0^{\theta_{max}} \frac{|4m^2 - \alpha_1 k_+^3|}{\omega(k_+,\alpha_1)} \\ &\times \frac{k\sin\theta d\theta}{|-k_+ + p\cos\theta - \frac{(1+\frac{3}{2}\alpha_1 k_+)}{\sqrt{1+\alpha_{(1)}k_+}}\sqrt{k_+^2 + E^2 - 2k_+ p\cos\theta}|}.\end{aligned} \tag{3.18}$$

A generalization of the vacuum Cherenkov radiation rate for any n is given by

$$\begin{aligned}\Gamma_{a\to a\gamma}^{(n)} =& \frac{e^2}{4\pi}\frac{1}{4E_a}\int_0^{\theta} \sum_{k_i} \frac{|4m_a^2 - \alpha_n k_i^{(n+2)}|}{\omega(k_i,\alpha_n)} \\ &\frac{k_i^2\sin\theta d\theta}{|p_a\cos\theta - k_i - \frac{(1+\frac{2+n}{2}\alpha_n k_i^n)}{\sqrt{1+\alpha_n k_i^n}}\sqrt{k_i^2 + E_a^2 - 2k_i p_a\cos\theta}|}\ \Theta(k_i),\end{aligned} \tag{3.19}$$

where k_i are the non zero photon momenta modes from the corrected energy-momenta conservation.

In figure 3.2, we show the emission rate for the three different models and proton mass, $m = m_p$, for this work, and due to the phenomenological considerations, we take the proton nuclei as spin 1/2 fermions. We have plotted, with a (green) dashed line, the modM emission rate at the first order from the expansion on E and $\tilde{\kappa}_{tr}$ from Eq. (3.3), setting $\tilde{\kappa}_{00} = 10^{-21}$, which is compatible with the limits reported in Ref. [27] . From a phenomenological point of view, the rate has four main characteristics. First, it has a growing behavior with charged particle energy. Second, it has a drop ending energy threshold for the model, inversely proportional to the LIV coefficient. This threshold protects the LI physics at energies below it. Third, for a given energy above the threshold, the emission rate decreases for smaller values in the LIV parameter. And fourth, it has a sensitive behavior with the mass and charge of the emitting particle. The last two characteristics will be discussed in the next section. In the dash-dotted (blue) line in the same figure, the MCS emission rate shows the same behavior as modM, but the derived threshold is higher in energy than the previous one since it is highly constrained from the M_{CS}. Finally, we present in a (red) continuous line the emission rate from the LIVgen1 model for very small θ and with a phenomenological threshold given by

$$E_a \gtrsim \left(\frac{4m_a^2}{\alpha_1}\right)^{1/3} . \tag{3.20}$$

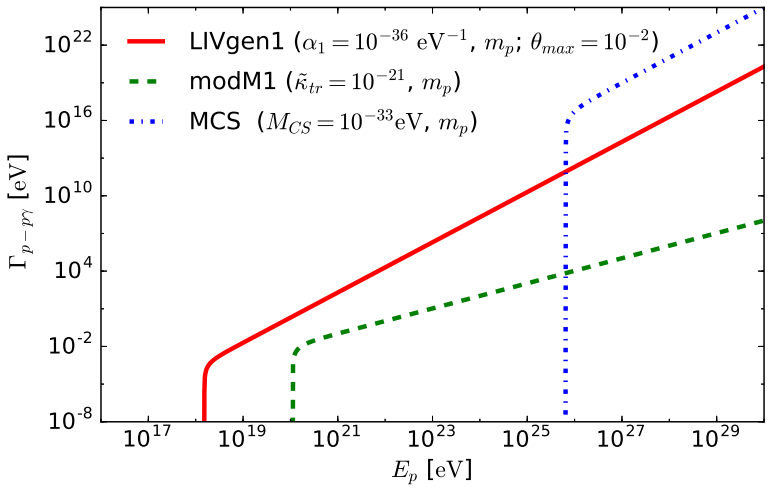

FIGURE 3.2: Comparison of emission rates for vacuum Cherenkov radiation for a proton. Free LIV parameters were chosen as indicated [24].

Last energy threshold can be motivated by the zero squared amplitude probability of the process, i.e. $4m_a^2 - \alpha_1 k_+^{(n+2)} = 0$, with $k_+ \sim E_a$ in the limit where $E_a, p_a \gg m_a$ and $\theta \to 0$. We have found that this phenomenological threshold removes the singularity in the rate at the threshold's region for UHECR's energies and beyond. For lower energies

about 10^{14} eV, further analysis is needed; in that region, the charged particle's mass-energy scale in the process, i.e., $m_a^2 \sim \alpha_n E_a^{n+2}$, is more appropriate to remove the singularity in the threshold region. Although, notice that the difference is a factor of 4.

In Fig. 3.3 we show the results for the case $n = 0$ and $n = 1$. The rates present a similar behaviour. In Fig. 3.4, the rates for different values of α_1 are presented. As shown, the energy threshold is higher for smaller values of α_1, the rates decrease as α_1 does, and for a given value of α_1, the rate grows with the energy.

Hence, as it can be appreciated in Figs. 3.2, 3.3 and 3.4, the generic approach reproduces the main features of the previous two models.

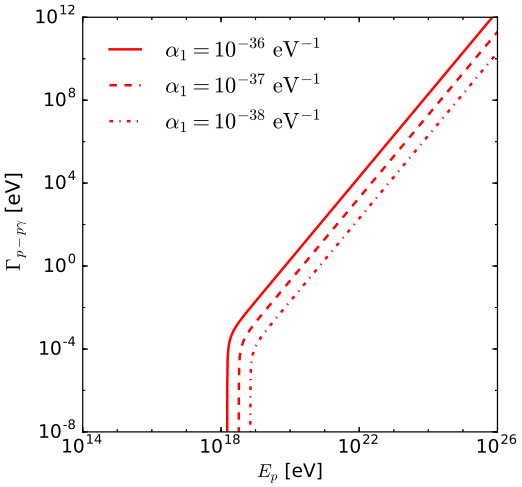

FIGURE 3.3: Emission rate for vacuum Cherenkov radiation for $n = 0, 1$, $m_a = m_p$ and $\theta_{max} = 10^{-2}$ [66].

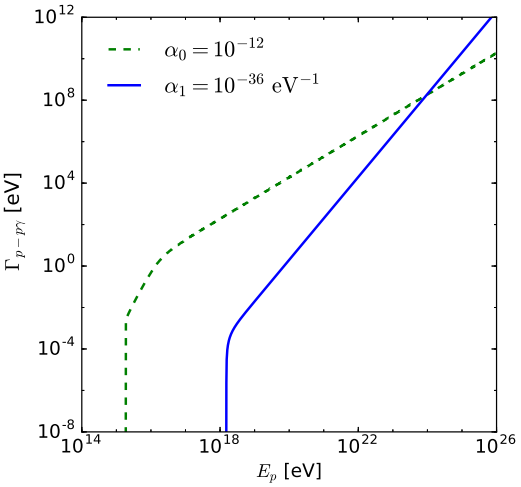

FIGURE 3.4: Emission rate for vacuum Cherenkov radiation for $n = 1$, $m_a = m_p$ and $\theta_{max} = 10^{-2}$ [67].

3.1.3 Sensitivity to UHECR mass composition

The present work, as mentioned before, aims to address the phenomenology derived from the LIV hypotheses to cosmic and gamma rays, so, considering the application of these models to the phenomenon of cosmic rays, we have chosen $m = m_p$ and $m = m_{Fe}$ as representative masses for a light and a heavy component of the cosmic ray flux, respectively. From section 2.2.1.1, it is estimated that the composition of ultra high energy cosmic rays (UHECR) is mixed between these two limits [68]. To appreciate the differences between them, in Figs. 3.5 and 3.6, the behavior of the Γ functions from LIVgen1 and modM for proton and iron nuclei are compared. From them, it can be seen that the effect of vacuum Cherenkov emission is sensitive to the composition of cosmic rays.

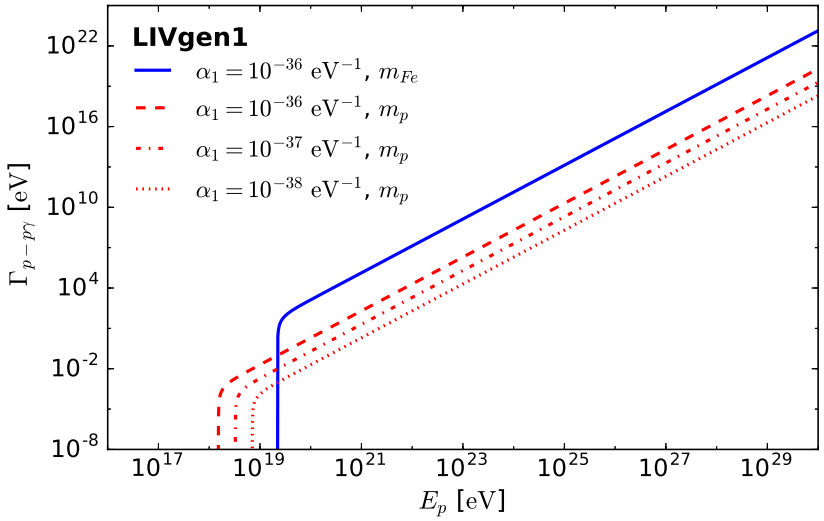

FIGURE 3.5: Emission rates for vacuum Cherenkov radiation from LIV generic approach at first-order correction, with $n = 1$ and $\theta_{max} = 10^{-2}$. Corresponding rates for m_{Fe}, m_p and different α_1 are as indicated. Both rates grow with energy, but lighter particles have a lower emission rate than heavier. The energy threshold is sensitive to particle composition [24].

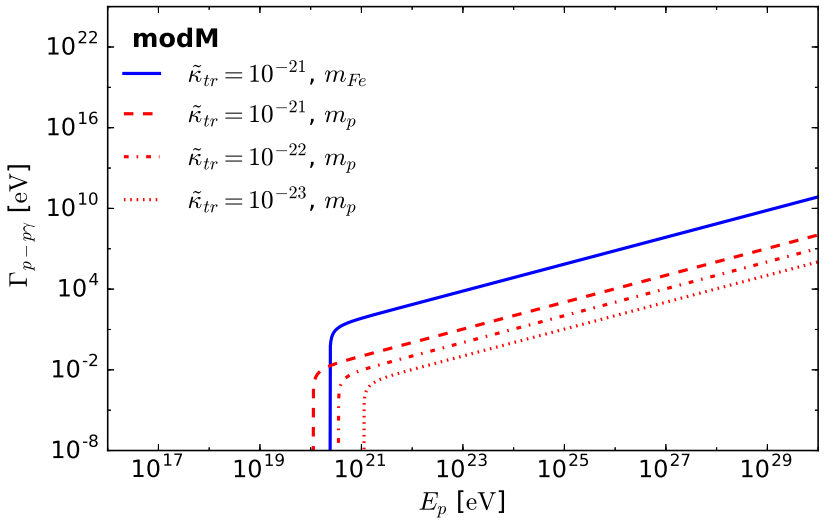

FIGURE 3.6: Emission rates for vacuum Cherenkov radiation from modified Maxwell theory. Corresponding rates for m_{Fe}, m_p and different $\widetilde{\kappa}_{tr}$ are as indicated. Both rates grow with energy, but lighter particles have a lower emission rate than heavier. The energy threshold is sensitive to particle composition [24].

In Figs. 3.5 and 3.6, we also plot the emission rate behaviour for smaller values in the LIV parameters to show that the emission rates become smaller as α_1 and $\widetilde{\kappa}_{tr}$ do.

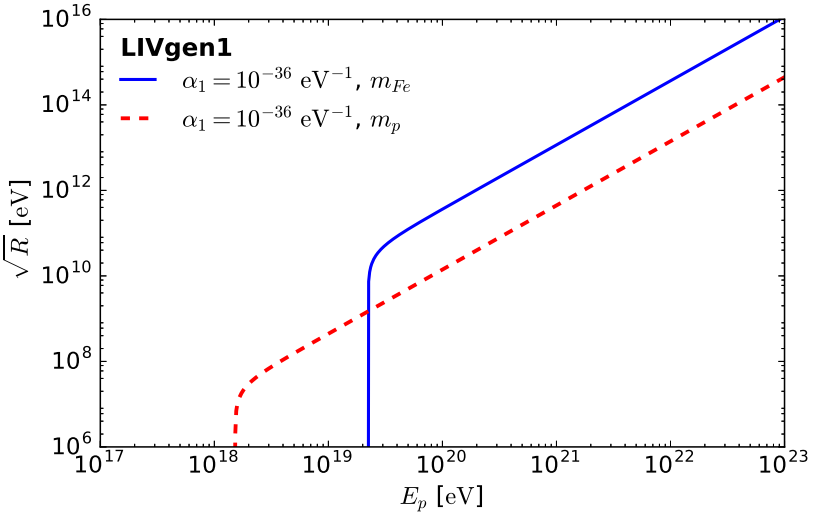

FIGURE 3.7: Radiated energy for vacuum Cherenkov radiation from LIV generic approach at first order correction, with $n = 1$ and $\theta_{max} = 10^{-2}$. Corresponding curves for m_{Fe} and m_p are as indicated [24].

In Fig. 3.7 it is shown the radiated energy from the generic approach, given by

$$R^2[\mathrm{eV}^2] = \frac{e^2}{4\pi}\frac{1}{4E}\int_0^{\theta_{max}} \frac{|4m^2 - \alpha_1 k_+^3|}{\omega(k_+,\alpha_1)} \times \frac{k_+^2 \sin\theta d\theta}{|-k_+ + p\cos\theta - \frac{(1+\frac{3}{2}\alpha_1 k_+)}{\sqrt{1+\alpha_{(1)}k_+}}\sqrt{k_+^2 + E^2 - 2k_+ p\cos\theta}|}. \tag{3.21}$$

As a consequence of this attenuation process, the models LIVgen1 and modM show an energetic region where vacuum Cherenkov radiation only affects the lighter nuclei but not the heavier, until the energy is high enough that vacuum Cherenkov radiation can attenuate all the massive nuclei simultaneously. In Fig. 3.8, we show the energetic region between the proton and iron nuclei threshold for different values of α_1. A reduction to the CR flux could be expected in this region due to vacuum Cherenkov radiation that starts with the lighter components and continues with more massive. Hence, the heavy components' tendency could be expected in the UHECR flux located between both thresholds. This effect is followed by a reduction in the contributions from the entire mass spectrum of CR at higher energies, where heavier nuclei are attenuated faster than lighter ones because heavier nuclei suffer vacuum Cherenkov attenuation some orders of magnitude higher than lighter nuclei in an energy scale where vacuum Cherenkov radiation is allowed simultaneously for the entire cosmic ray mass spectrum, between proton and iron limits, and heavier nuclei will be attenuated sooner in their propagation. This special behavior is clarified in Fig. 3.9 with the first emission probability as a function of mean free path.

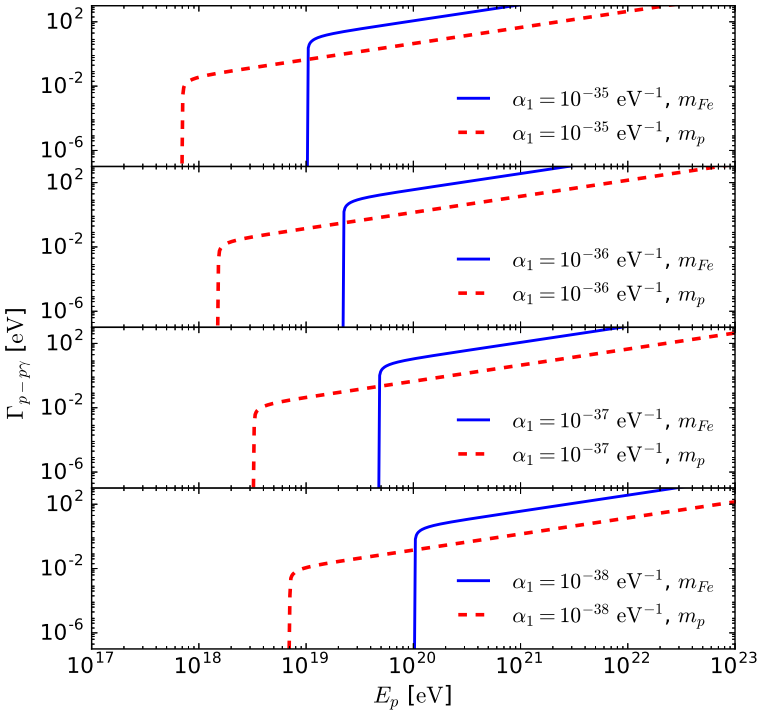

FIGURE 3.8: Vacuum Cherenkov energetic region, between proton and iron nuclei threshold, for different values of α_1. A reduction to the CR flux could be expected in this region due to vacuum Cherenkov radiation that starts with the lighter components and continues with heavier.

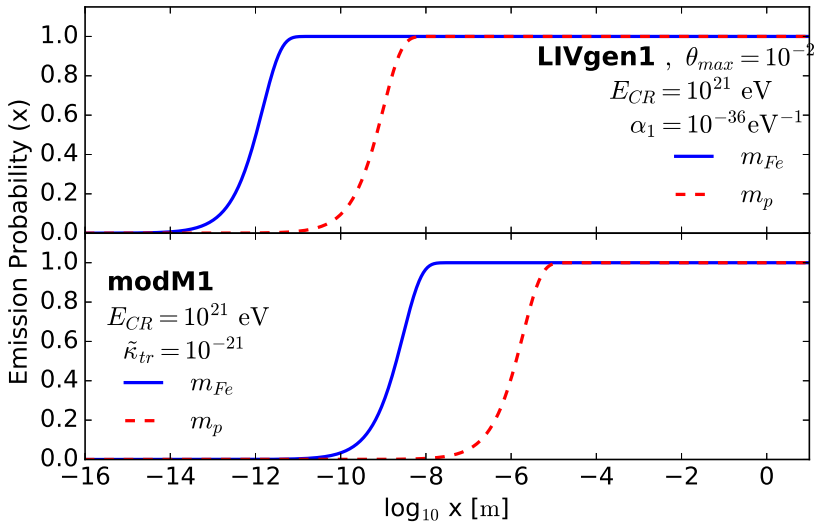

FIGURE 3.9: Vacuum Cherenkov first emission probability from modified Maxwell theory and LIV generic approach at first-order correction [24].

From the results in Figures 3.5, 3.7 and 3.9, and for a value of the LIV photon parameter, $\alpha_1 = 10^{-36} eV^{-1}$, one could expect that this trend would show up around an energy range of about 10^{18} to 10^{19} eV. UHECR observatories such as Pierre Auger, Telescope Array, and HiRes have measured and reported the spectrum of ultra-energy cosmic rays at EeV energies [69–71]. Thus, a dedicated analysis with their data could probe such an effect or set limits to α_n.

Chapter 4

Photon Decay

In the same way that spontaneous photon emission, photon decay, as depicted in Fig. 4.1, is kinematically allowed by LIV-hypothesis. This special LIV process has been studied before in the context of generic LIV corrections and the SME (see for instance [12, 18–20, 23, 35, 64]).

In the present chapter, we derive the LIV photon decay rate following the generic construction developed and validated in the previous chapter 3. It was shown that such approximation preserves the generalities of the particular models presented in section 2.1.4 and derived from the SME. The results achieved in this chapter show that photon decay derives in a very restrictive scenario for the highest energy photons [23], especially for those propagating from astrophysical sources. Therefore, it is possible to attain tight upper limits for the photon sector's generic LIV coefficient by using the highest photon energy astrophysical measurements.

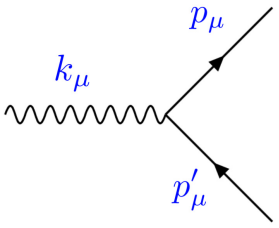

FIGURE 4.1: Feynman diagram for LIV photon decay to a pair of leptons.

4.1 LIVgen1 decay rate for any order n

As we previously did for vacuum Cherenkov radiation, we start the present analysis by considering the LIV photon dispersion relation in Eq. (3.6), $\omega^2 = k^2(1 + \alpha_n k^n)$. The decay rate of the process will be thus given by

$$d\Gamma = \frac{s}{2}\frac{1}{\omega(k,n,\alpha_n)}|\mathcal{M}|^2\frac{d^3p}{(2\pi)^3 2E(p)}\frac{d^3p'}{(2\pi)^3 2E'(p')} \times (2\pi)^4\delta^{(4)}(k-p-p')\ \Theta(p), \tag{4.1}$$

where $(E, \mathbf{p})$ and $(E', \mathbf{p}')$ are the four momenta components of the final leptons, l^+ and l^-, respectively. The squared probability amplitude is then given by Eq. (3.11) from the previous section. Next, we shall perform the integration over p' and write the delta function as follows,

$$\begin{aligned}\delta^{(0)}\left(g(k,p,m,n,\alpha,\sin\theta)\right) = &\delta^{(0)}\Big(\ \sqrt{1+\alpha_n k^n}\ k \\ &- \sqrt{p^2+m^2} - \sqrt{p^2+k^2+m^2-2pk\cos\theta}\ \Big)\ .\end{aligned} \tag{4.2}$$

As before, we use the g function roots, now given by the expression,

$$(\alpha_n k^n + 2\sin^2\theta)p^2 - 2\alpha_n k^{n+1}\cos\theta\ p + 2m^2 + \alpha_n k^n m^2 = 0. \tag{4.3}$$

Notice that unlike the expressions obtained for the previous process, Eq. (4.3) is a second order polynomial function in p. In order to solve it, the condition $k \neq 0$ is assumed. It is not difficult to show that p will satisfy energy-momentum conservation when,

$$\begin{aligned}p_\pm = &\Big(\alpha_n k^{n+1}\cos\theta \pm \sqrt{\alpha_n^2 k^{2n+2}\cos^2\theta - 4(\sin^2\theta + \alpha_n k^n)(1+\alpha_n k^n)m^2}\Big) \\ &\times (2\alpha_n k^n + 2\sin^2\theta)^{-1}.\end{aligned} \tag{4.4}$$

In order to ask for p to be real and positive, the discriminant in Eq. (4.4) must be real and positive too. This condition restricts the possible emission angles for any given momentum of the photon to the LIV parameters. To exemplify this restriction, we have plotted the discriminant behavior for a photon energy of 100 TeV, for $m = m_e$, $n = 1$ and different values of α_1. The result is depicted in Fig. 4.2. Due to the angular dependence of the function, while α_1 decreases, the discriminant becomes negative for a given interval in θ, and the permitted integration region decreases. In the limit when θ goes to zero, the angular integration space becomes null, and the process is forbidden.

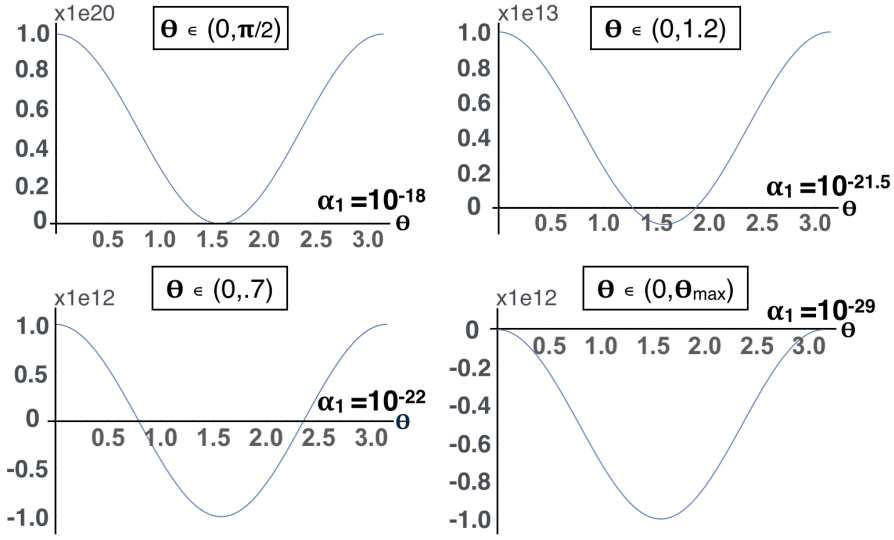

FIGURE 4.2: The discriminant behavior from Eq. (4.4) for $k = 100$ TeV, $m = m_e$, $n = 1$ and different values of α_1 in eV^{-1} units. The positive region set the integration limits for the decay rate in Eq. (4.6). θ is in radian units [24].

This limit can be parametrized to set a threshold on α_n, above which LIV photon decay process is enabled,

$$\alpha_n \geq \frac{4m^2}{k^n(k^2 - 4m^2)}. \tag{4.5}$$

Using the expressions in Eqs. (3.6), (3.11) and that for $p_\pm$ in Eq. (4.4), to perform the integral over p, the analytic expression for the photon decay rate Γ, in the LIV generic approach at first order in α_n (LIVgen1), is

$$\Gamma^{(n)}_{\gamma\to l^-l^+} = \frac{e^2}{4\pi}\frac{|4m^2 - \alpha_n k^{n+2}|}{4k\sqrt{1+\alpha_n k^n}} \times \int_0^{\theta_{max}} \sum_{p_\pm} \frac{p^2 \sin\theta d\theta}{|pE' + (p - k\cos\theta)E|}, \tag{4.6}$$

where

$$E = \sqrt{p^2 + m^2}, \quad E' = \sqrt{k^2 + p^2 + m^2 - 2kp\cos\theta}. \tag{4.7}$$

Numerically by solving the integral for $n = 1, 2$, we find the decay rate shown in Fig. 4.3. It can be appreciated that the decay rates are steadily growing with the energy for both $n = 1, 2$. They show a change in the slope at energy inversely proportional to the LIV coefficient α_n, and the decay rates become smaller as α_n does. We have found that the case n=0 have a similar behaviour than for $n = 1, 2$ as it can be seen in Fig. 4.4 [67]. In addition, Eqs. (4.5), (4.6), for n=0, are compatible, under the assumption that LIV corrections are made only in the photon sector, with the threshold and the decay rate reported in Ref. [12].

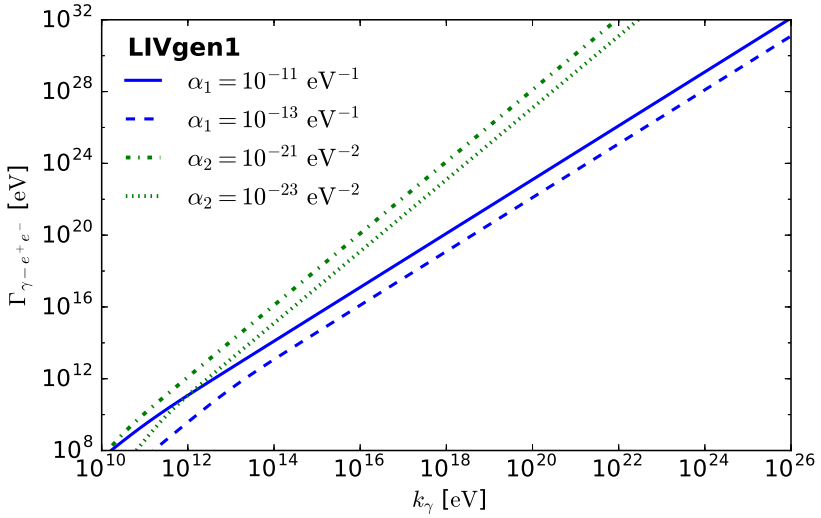

FIGURE 4.3: Photon decay rates from LIV generic approach for $n = 1, 2$ and $\theta_{max} \approx \pi/2$. α_1 is in eV^{-1} units [24].

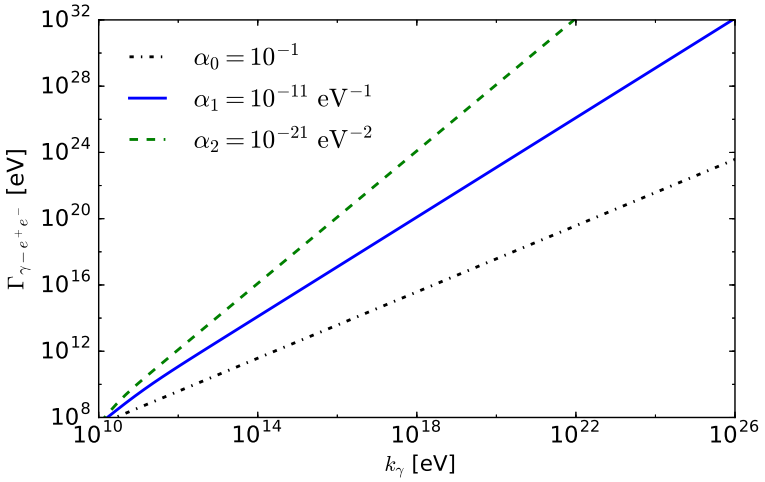

FIGURE 4.4: Decay rate for LIV photon decay into electron positron pairs, for n=0,1, and 2. α_1 is in eV^{-1} units [67].

As an example, to illustrate how restrictive this process is, in Fig. 4.5 we show the photon survival probability as a function of the mean free path for photons. There we have used the same values we used in Fig. 4.2. From these results, it is clear that a 100 TeV photon will not be able to propagate beyond $\sim 10^{-12}$ m, for an $\alpha_1 = 10^{-18}\ eV^{-1}$, that is a non-restrictive value for current limits (see table 2.2). However, in the limit, where $\theta_{max} \to 0$, an astrophysical photon of 100 TeV will be able to reach Earth from kpc distances, but a smaller α_n is implied.

This would set a critical value that fixes an energy-dependent threshold for the LIV parameter. For any α_n above threshold in Eq. (4.5), photon decay becomes extremely efficient. On the other hand, below the threshold, the process is forbidden. So, using

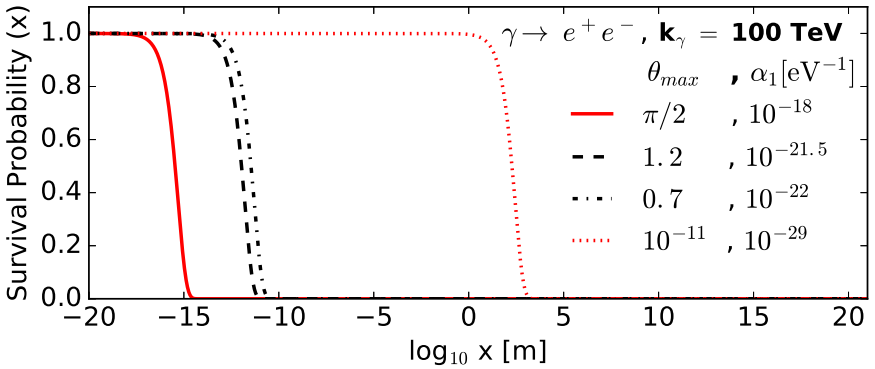

FIGURE 4.5: Photon decay probability as a function of the mean free path, for a 100 TeV photon and for the integration limits in Fig. α_1 is in eV^{-1} units. 4.2 [24].

the following parametrization, $E_{QG}^{(n)} \approx 1/\alpha_n^{1/n}$, Eq. (4.5) becomes,

$$E_{QG}^{(n)} > k_{obs} \left[\frac{k_{obs}^2 - 4m^2}{4m^2} \right]^{1/n} . \tag{4.8}$$

That means that a lower limit for $E_{QG}^{(n)}$ in the photon sector will directly emerge from any observed high energy cosmic photon event of momentum k_{obs}. That is one of the main results of this thesis.

4.2 Limits on $E_{QG}^{(1,2)}$

Following this line of thought, and using above expression for photon decay into electron positron pairs, $m = m_e$, we can depict the $E_{QG}^{(n)}$ limit as a function of the photon energy event, as it can be seen in Fig. 4.6, for $n = 1$ and Fig. 4.7 for $n = 2$, represented by the (blue) diagonal line on the plots. The (red) continuous and horizontal line in both figures is one of the best limits for the LIV generic photon sector proposed by *Fermi*-LAT in 2013 [14] (For a shortlist of lower limits, see Tab. 2.2). The dot-dashed and dashed (red) lines are our derived limits from H.E.S.S. and HEGRA reported data [27, 35, 59, 60, 62]. The (colored) bars are the uncertainties of the highest photon energy reported and presented in sections 2.2.2.1 and 2.2.2.2. We are using the lower value as observed photon energy from astrophysical distances. In our analysis, the best limits are obtained from HEGRA data, as indicated in the figures. We found that $E_{QG}^{(1)} \geq 1.5 \times 10^{20} GeV$ and $E_{QG}^{(2)} \geq 2.8 \times 10^{12} GeV$, for $n = 1$ and $n = 2$, respectively.

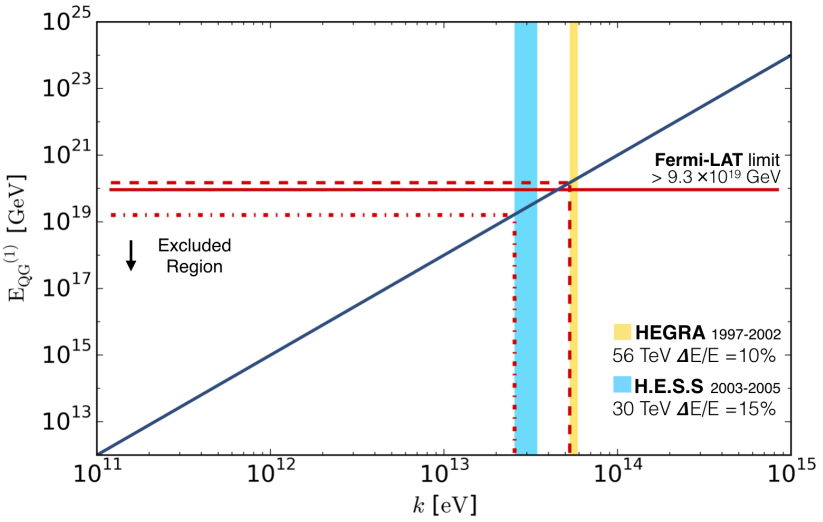

FIGURE 4.6: $E_{QG}^{(1)}$ excluded energy region by LIV photon decay into electron-positron pairs with HEGRA [27, 62] and H.E.S.S. [35, 59] photon energy measurements. Using Eq. (4.5) we found that $E_{QG}^{(1)} \geq 1.5 \times 10^{20} GeV$ by HEGRA and $E_{QG}^{(1)} \geq 1.7 \times 10^{19} GeV$ by H.E.S.S., in the $n = 1$ case [24].

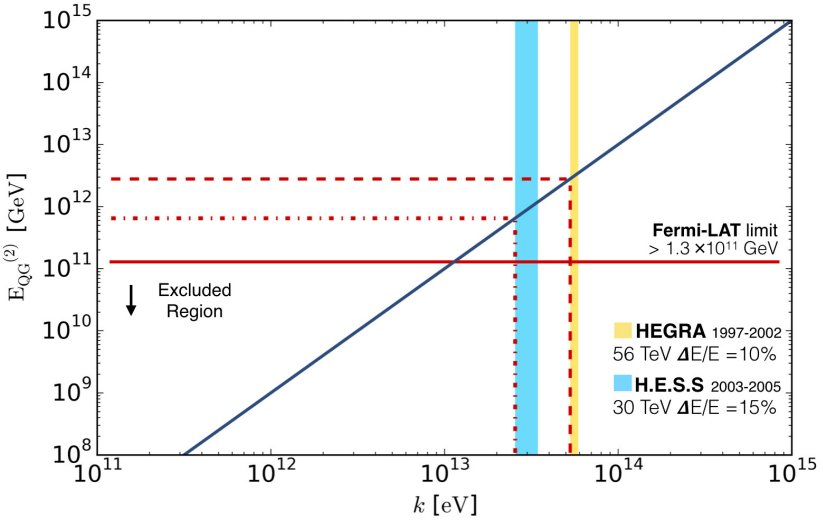

FIGURE 4.7: $E_{QG}^{(2)}$ excluded region by LIV photon decay into electron-positron pairs with HEGRA [27, 62] and H.E.S.S. [35, 59] photon energy measurements. Using Eq. (4.5) we found that $E_{QG}^{(2)} \geq 2.8 \times 10^{12} GeV$ by HEGRA and $E_{QG}^{(2)} \geq 6.5 \times 10^{11} GeV$ by H.E.S.S., in the $n = 2$ case [24].

Chapter 5

Cosmic ray photoproduction processes

In the previous chapters, we studied processes that could not be achieved from a LI theory, and we analyzed the derived phenomenology for cosmic and gamma rays. However, LIV-derived physics has consequences in known processes, which can manifest themselves as small corrections to their expected physics and grow with the energy. This is the case of the production threshold shift effect for standard processes.

In this thesis's spirit, we will focus on corrections produced by the generic modification to the particle dispersion relations, especially on those with a particular interest in cosmic and gamma rays.

Previous studies can be found in Refs. [19, 21, 22]. However, there is also an interesting feature derived from this approach that we believe deserves further attention and which is presented in here. To this aim, in the current chapter, we develop a generalization of the LIV threshold equations, which parametrize the shift from the LI expected threshold. As we discuss later, in the generic LIV setup, a higher energy threshold appears where particle production becomes again forbidden. In the scenario where the collision describes the interaction of an energetic particle propagating in the cosmic photon background, this last threshold means that at some high energy, the cosmic particle shall again freely propagate, at least free from this particular process; this motivates us to call it a recovery scenario.

5.1 Generalized LIV-threshold equation

Let be a process of the type

$$\text{A B} \quad \rightarrow \quad \text{C D}, \tag{5.1}$$

in which in a LI regime, the massive final particle states C and D, require some minimal energy from the initial particles A and B for the process to happen.

Now, we apply, in the most general way to all involved particles of the process in Eq. (5.1), the modification to their dispersion relation, as presented in Eq. (2.24).

For this work and in order to be specific, we have chosen two representative and relevant processes for cosmic and gamma-ray physics: pion photoproduction and pair photoproduction [40, 46, 47, 72],

$$p_{CR} \quad \gamma_b \longrightarrow p \quad \pi^0, \tag{5.2}$$

$$\gamma_{CR} \quad \gamma_b \longrightarrow e^+ e^-, \tag{5.3}$$

where b and CR denote background and cosmic ray primary particles, respectively. Notice that we have chosen protons for the first process, but the analysis would be equally valid for neutrons too. Similar approaches can be found in Refs. [19, 21, 22]. Furthermore, we shall consider a first-order correction function Ξ to energy-momentum conservation to explore the relevance at cosmic ray energies. This correction is motivated by the work in Ref. [73], where several LIV coefficients were added in order to properly correct energy-momenta. However, for an alternative model, see also [74]. To the best of our knowledge, such a general approach has not been explored in this general context elsewhere before.

5.1.1 Pair photoproduction LIV-threshold relation

In order to motivate the LIV-threshold equation for the general case, we first present the case of pair photoproduction in Eq. (5.3), so, let (ω, ω_b) and (E_+, E_-) be the corresponding initial and final energies of particles in the process. Therefore, in the LIV setup, we write energy conservation relation as

$$E_+ + E_- = \omega + \omega_b + \Xi. \tag{5.4}$$

Or equivalently,

$$E_+ = K(\omega + \omega_b + \Xi), \tag{5.5}$$

and

$$E_- = (1 - K)(\omega + \omega_b + \Xi), \tag{5.6}$$

where K is the inelasticity function of the process.

The following considerations are also taken in this analysis:

- The system is that where the collision can be assumed head-on.
- The final momenta could be taken collinear since the very high and ultra high energy cosmic photons have higher energy than the photon background, $\omega_b \ll \omega$.
- The ultra-relativistic regime approximation can be used, that is $m \ll \{E, p\} \ll M$. Where M is the energy scale associated with the LIV physics.
- We keep only first order in the LIV coefficients since they are expected to be small; hence, any product of them can be neglected.
- The LIV parameters, in general, are considered not universal.

Then, for pair photoproduction, let the invariants be

$$S_{photon} = \omega^2 - k^2 = -\alpha_n \omega^{n+2}, \tag{5.7}$$

and

$$S_{\pm} = E_{\pm}^2 - p_{\pm}^2 = m_e^2 - \alpha_{\pm,n} E_{\pm}^{n+2}, \tag{5.8}$$

where we have inserted a different LIV parameter for the electron sector to account for a possible particle dependence. A previous work has studied similar corrections but considering a momenta correction with the opposite sign in α_n [19].

Substituting and equating the initial and final invariant, we found that

$$\begin{aligned} & 4\omega\omega_b - m_e^2 \left(\frac{1}{K(1-K)} - \frac{m_e^2}{2K(1-K)(\omega+\omega_b+\Xi)^2} \right) \\ = \; & \alpha_n \omega^{n+2} \left[1 + \frac{\omega_b^{n+2}}{\omega^{n+2}} - \frac{\omega_b}{\omega} \left(1 + \frac{\omega_b^n}{\omega^n} \right) \right] \\ & + \alpha_{+,n} K^{n+1} (\omega+\omega_b)^{n+2} \times \left[-1 + \frac{m_e^2}{2} \frac{1}{(1-K)(\omega+\omega_b)^2} \right] \\ & + \alpha_{-,n} (1-K)^{n+1} (\omega+\omega_b)^{n+2} \times \left[-1 + \frac{m_e^2}{2} \frac{1}{K(\omega+\omega_b)^2} \right] . \end{aligned} \tag{5.9}$$

Note that Ξ, the LIV contribution to energy-momenta conservation, was reduced to one term. By demanding that $m_e,\ \omega_b,\ \Xi \ \ll \omega$, the last expression becomes, at the lowest correction order,

$$4\omega\omega_b - \frac{m_e^2}{K(1-K)} = \beta_n \omega^{n+2} \ , \tag{5.10}$$

where we have defined

$$\beta_n = \alpha_n - \alpha_{+,n} K^{n+1} - \alpha_{-,n} (1-K)^{n+1} \ . \tag{5.11}$$

Notice that the contribution of Ξ has disappeared. This clearly shows that, at leading order, LI momentum conservation rule effectively holds for high energy cosmic particle collisions.

In the limit where $\alpha_n = \alpha_{\pm,n} = 0$, the RHS of Eq. (5.10) vanishes, thus providing a unique solution to ω in terms of K, given by $\omega_0 = \frac{m_e^2}{4K(1-K)\omega_b}$. For $K = 1/2$, the standard LI pair production threshold for a cosmic photon will arrive as usual, where

$$\omega_{th}^{LI} = \frac{m_e^2}{\omega_b} \ . \tag{5.12}$$

Otherwise, Eq. (5.10) is a polynomial equation of order $n+2$ on ω, which in general may have more than one real solution. This shall be the core of our argument below. It is instructive to rewrite Eq. (5.10) in a more generic and straightforward form by defining the dimensionless variables

$$x_\gamma = \frac{\omega}{\omega_0} \quad \text{and} \quad \Lambda_{n,\gamma} = \frac{\omega_0^{n+1}}{4\omega_b}\beta_n \ . \tag{5.13}$$

In such terms the polynomial threshold equation for pair photoproduction becomes

$$\Lambda_{n,\gamma} x_\gamma^{n+2} - x_\gamma + 1 = 0 \ . \tag{5.14}$$

The last equation is consistent with the result presented in Ref. [19] for pair production under a generic LIV correction and assuming LI energy-momentum conservation.

5.1.2 General photoproduction LIV-threshold relation

Now we proceed with the general photoproduction process case

$$A\ \omega_b \quad \rightarrow \quad C\ D \ ,$$

to determine its corresponding threshold equation. Particular cases will be pair and pion photoproduction by cosmic nucleons. Following a similar path as before, we would start by writing down the corresponding modified dispersion relations for the involved particles. Aside to Eq. (5.7) for the background photon, we would also have

$$E_i^2 - p_i^2 = -\alpha_{i,n} E_i^{n+2},$$

for $i = A, C, D$, respectively.

Once again, we consider the same approximated conditions as in the pair photoproduction case.

Thus, by developing a similar algebra as in previous section we found the following **LIV-threshold equation**, at the lowest order and for high energy cosmic ray primaries,

$$4\omega_b E_A + m_A^2 - \frac{Km_C^2 + (1-K)m_D^2}{K(1-K)} = \Upsilon_n E_A^{n+2} \ , \tag{5.15}$$

where, assuming that $\omega_b \ll E_A$,

$$\Upsilon_n = \alpha_{A,n} - \alpha_{D,n}K^{n+1} - \alpha_{C,n}(1-K)^{n+1} \ . \tag{5.16}$$

Note that, Eq. (5.16), parametrizes the **LIV-correction**, and if we set all LIV coefficients to zero, Eq. (5.15) implies the solution

$$E_{A0} = \frac{Km_C^2 + (1-K)m_D^2}{4\omega_b K(1-K)} - \frac{m_A^2}{4\omega_b} \ , \tag{5.17}$$

which is the expected **LI-threshold equation**.

Once more, by introducing dimensionless variables in the general case, now given by

$$x_A = \frac{E_A}{E_{A0}} \quad \text{and} \quad \Lambda_{n,A} = \frac{E_{A0}^{n+1}}{4\omega_b}\Upsilon_n \ , \tag{5.18}$$

we finally get the same form for the threshold equation as in the pair photo-production case. Therefore, irrespective of the process, we can express such an equation as

$$\Lambda_n x^{n+2} - x + 1 = 0, \tag{5.19}$$

where in general $x = E^{LIV}/E_{th}^{IL}$ and Λ_n contains an energy independent linear function, $\{\beta_n, \Upsilon_n\}$, depending on all LIV parameters. Clearly, if $\{\beta_n, \Upsilon_n\} = 0$, LI regime would be recovered.

It is worth stressing that in both the cases, Eq. (5.19) is, to first approximation in LIV terms, independent from particle nature, the functional form of A in Eq. (2.24) and Ξ in Eq. (5.4). Last means that the results do not depend on linear corrections to the energy-momentum laws.

5.1.2.1 Particular cases

Pair photoproduction: $\gamma_{CR} \;\; \gamma_b \longrightarrow e^+e^-$

The particular results derived in section 5.1.1 for pair photoproduction are clearly recovered from the general expressions, if one takes

$$m_A = 0, \quad \text{and} \quad m_{C,D} = m_e.$$

Specifically, Eqs. (5.15) and (5.16), take the form of Eqs. (5.10) and (5.11), which for illustrative purpose, here we write them again,

$$4\omega\omega_b - \frac{m_e^2}{K(1-K)} = \beta_n \omega^{n+2} \ ,$$

where

$$\beta_n = \alpha_n - \alpha_{+,n}K^{n+1} - \alpha_{-,n}(1-K)^{n+1} \ .$$

These expressions are the LIV-threshold equation for pair photoproduction and the LIV contribution's parametrization by each particle involved in the process. Additionally, from Eq. (5.18), we write the expected LI-threshold for a high energy photon to produce a pair $e^{\pm}$ by interaction with the background as

$$\omega_0 = \frac{Km_e^2 + (1-K)m_e^2}{4\omega_b K(1-K)}. \tag{5.20}$$

In Ref. [75], LIV threshold shifts in pair photoproduction are considered in the calculations of photon propagation in the Universe. The corresponding photon horizon, including LIV effects, is studied and used to predict significant changes in photons' propagation with energy above $10^{16}eV$.

Pion photoproduction: $p_{CR} \;\; \gamma_b \longrightarrow p \;\; \pi^0$

Now, by taking

$$m_{A,C} = m_p \quad \text{for a proton,}$$

$$m_D = m_\pi \quad \text{for a pion}$$

Eqs. (5.15), (5.16) and (5.18), become,

$$4\omega_b E_p + m_A^2 - \frac{Km_p^2 + (1-K)m_\pi^2}{K(1-K)} = \Upsilon_n E_p^{n+2} \ , \tag{5.21}$$

where

$$\Upsilon_n = \alpha_{p,n} - \alpha_{\pi,n}K^{n+1} - \alpha_{p,n}(1-K)^{n+1} \ . \tag{5.22}$$

Eqs. (5.22) is the LIV parametrization of all the LIV coefficients involved in the process, into the LIV-threshold equation for pion photoproduction in Eq. (5.21).

Finally, using the result in Eq. (5.18), the expected proton energy threshold in a LI theory is given by

$$E_{p_0} = \frac{Km_p^2 + (1-K)m_\pi^2}{4\omega_b K(1-K)} - \frac{m_p^2}{4\omega_b} \,. \tag{5.23}$$

and if we set $K = \frac{m_\pi}{m_\pi + m_p}$, we get the known LI threshold for neutral pion photoproduction,

$$E_{p_0} = \frac{m_\pi^2 + 2m_\pi m_p}{4\omega_b} \,. \tag{5.24}$$

This particular threshold plays a relevant role in UHECR since the end of CR flux is commonly associated with the GZK cutoff [40, 46, 47] generated from this threshold.

5.2 The LIV secondary threshold

Let us next consider the implications of the LIV threshold equation (5.19). Clearly, to each value of Λ_n it shall correspond a different scenario that describes the behavior of photoproduction processes. For simplicity, we take the lower order correction, $n = 1$, and then comment on the general case. In this case, we get the cubic equation

$$f(x) = \Lambda_1 x^3 - x + 1 = 0,$$

which in general has three different solutions, but setting $\Lambda_1 = 0$ the LI case is recovered. As it is easy to check, the possible roots of $f(x)$ provide three different physical scenarios that can be seen in Fig. 5.1, and are described as follows

i) $\Lambda_1 < 0$. In this scenario, there is only one real root for $f(x)$, and the other two roots are complex, and thus, nonphysical. Furthermore, the real root turns out to be always positive but smaller than one. This implies that the derived LIV physics produces a threshold at lower energies than expected in the LI regime. ($E_{th}^{LIV} < E_{th}^{LI}$). This means an earlier activation of photoproduction in energy than expected. The gap between the two thresholds will increase as Λ_1 goes to smaller values.

   Note that for an universal α_1 we get $\beta_1 = \Upsilon_1 = \alpha_1 K(2-K)$, and thus this scenario only arises provided that $\alpha_1 < 0$.

ii) There is a critical value at $\Lambda_1 = 4/27$ above, which $f(x)$ has only one negative and two complex roots. Therefore, for $\Lambda_1 > 4/27$, there is no physical solution to the

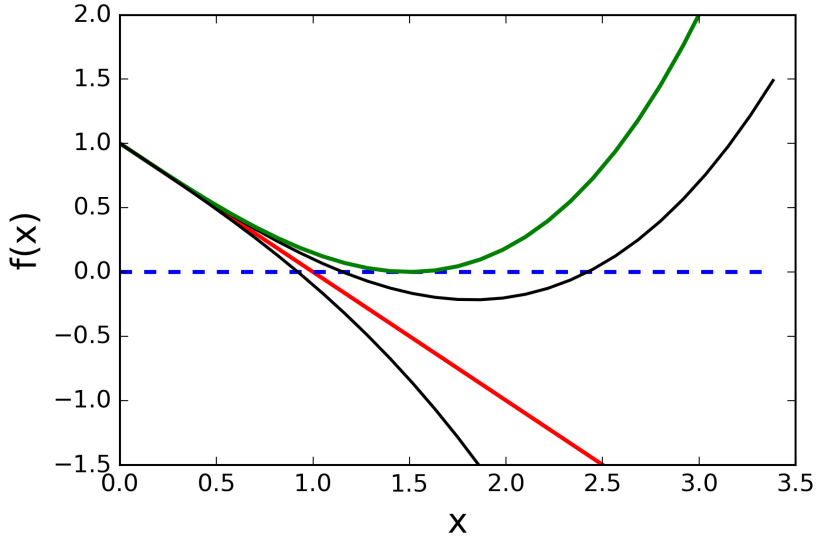

FIGURE 5.1: $f(x)$ for $n = 1$ and different values of Λ_1. The dashed (blue) line is $f(x) = 0$. From bottom to top, the continuous lines are $\Lambda_1 = -0.1, 0, 0.1$ and $\Lambda_{\rm nc}$ (green). The LI scenario corresponds to the continuous (red) line where $\Lambda_1 = 0$.

threshold equation. Consequently, the photoproduction process becomes forbidden, and the Universe gets transparent to propagate the cosmic ray primary. Such a scenario is, of course, in direct contradiction with astrophysical observations, and thus, one must impose the consistency condition

$$\Lambda_1 < 4/27. \tag{5.25}$$

Note that such a critical value do exist for any arbitrary n.

A simple algebra shows that, if $f(x) = \Lambda_n x^{n+2} - x + 1 = 0$, hence, there is an extremal point, x_{nc}, that satisfies $f'(x_{nc}) = 0$, which implies that

$$\Lambda_n \; x_{nc}^{n+1} = \frac{1}{(n+2)}. \tag{5.26}$$

However, if x_{nc} is a root of $f(x)$, thus $f(x_{nc}) = 0$. That is,

$$\begin{aligned} f(x_{nc}) &= \Lambda_n x_{nc}^{(n+1)} x_{nc} - x_{nc} + 1 = 0, \\ &= \frac{1}{(n+2)} x_{nc} - x_{nc} + 1 = 0, \\ &= \frac{1-2-n}{(n+2)} x_{nc} + 1 = 0, \\ &= -\frac{(n+1}{(n+2)} x_{nc} + 1 = 0. \end{aligned}$$

So, the only root is given by

$$x_{nc} = \frac{(n+2}{(n+1)}. \tag{5.27}$$

Using the critical value, x_{nc}, in Eq. (5.26),

$$\Lambda_{nc} = \frac{(n+1)^{n+1}}{(n+2)^{n+2}}. \tag{5.28}$$

Real roots demands that $\Lambda_n < \Lambda_{nc}$, which is a quickly decreasing function of n. And at critical value, the only root is x_{nc}.

iii) Finally, for $0 < \Lambda_1 < 4/27$ the threshold equation has three real solutions. Nevertheless, only two of them are positive, and physically acceptable. A nontrivial but important consequence arises here. A range of x values shall now become bounded by two thresholds.

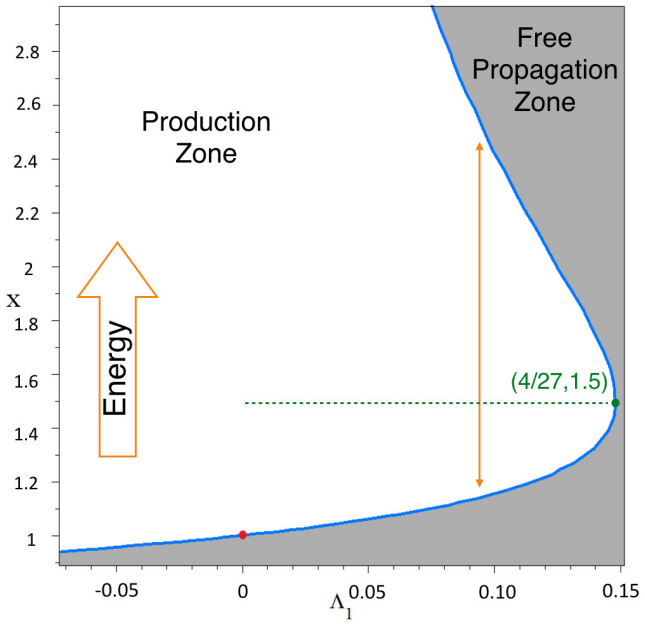

FIGURE 5.2: Solutions to the threshold equation for $n = 1$, as a function of Λ_1. The $f(x)$ roots separate free propagation and photoproduction zones as indicated. Critical point (in green) indicates the upper limit on Λ_1. LI case is stressed by a (red) point at $\Lambda_1 = 0$ [24].

These scenarios' whole effect can easily be understood if we plot $f(x)$ roots as a function of Λ_1, as we have done in Fig. 5.2, and notice that the corresponding curve divides the parameter space into two regions. Clearly, by merely looking at the particular solution where LI holds (for $\Lambda_1 = 0$), we can identify the free propagation zone below the curve (where $E < E_{th}$). This zone is analytically connected to the region on the RHS of the plot, where $\Lambda_1 > 4/27$, according to our previous discussion. Furthermore,

it is connected to the region above the curve, where $0 < \Lambda_1 < 4/27$. The conclusion is unavoidable. Whereas the lowest root gives the expected energy threshold where photoproduction gets switched on, the second root, at higher energies, represents a new energy threshold where photoproduction shall, once more, stop.

These conclusions are consistent with the findings in Ref.[19] for pair photoproduction, although it is worth stressing that this physics is rather common to all photoproduction processes. Furthermore, it is not difficult to realize that there always exists a secondary threshold for any value of n, and for $0 < \Lambda_n < \Lambda_{nc}$. As a matter of fact, RHS of Eq. (5.19) has a linear behavior for small x, with a negative slope, whereas, for large x, it is dominated by the single term $\Lambda_n x^{n+2}$, with a positive derivative. Accordingly, there exists a single absolute minimum, at $x_{min} = [(n+2)\Lambda_n]^{-1/n+1}$, that lays in the energy region where photoproduction is on, beyond the first root (above the first threshold). This, in turn, gives rise to a second root, and therefore, to the second threshold. That would be the signature of the generic LIV for any photo production process.

This phenomenon would produce an *opacity band* for a propagating primary. Out of the band, ultra high energy cosmic ray particles, like protons and very high energy photons, would be free of the photoproduction processes produced by the interactions with background photons. Additionally, the bandwidth decreases for larger values of Λ_n. Whereas the first threshold can only take values from $x \in [1, x_{nc})$, the second threshold decreases very fast as Λ_n grows, until the photoproduction processes fade out when Λ_n reaches its critical limit, Λ_{nc}.

The appearance of an opacity band should have visible effects in the integrated cosmic ray flux. Although a detailed calculation of this is out of the present work scope, our results suggest that potentially visible effects are possible. On general grounds, for individual particles, one would expect that the physics should be very similar to the standard LI scenario for cosmic ray primaries with energies within the band. Photoproduction processes will contribute to quickly diminishing the proton primary's energy and the disappearance of high energy primary photons. However, if energies well above the second threshold were accessible to the primaries, they will see a transparent universe along with its propagation, which means no depletion on their flux would be expected. In this sense, the measured flux would show a recovery behavior at the largest energies.

Physical implications of the purely LIV secondary threshold are interesting. A cosmic particle primary shall encounter an opaque universe and its propagation, due to photon background, only for primary energies within the two thresholds. At such energies, photoproduction will attenuate the particle's energy, moving it to lower values where the process is switched off, permitting further free propagation. Of course, this is generally the standard LI scenario, but for the shifting of the actual position of the threshold. On

the other hand, if astrophysical sources injected particle primaries at energies well above the LIV secondary threshold, they would not suffer attenuation due to photoproduction. Recovery on the cosmic particle's primary flux would be expected as a consequence above the opacity band defined by the thresholds.

5.2.1 The Pion photoproduction case

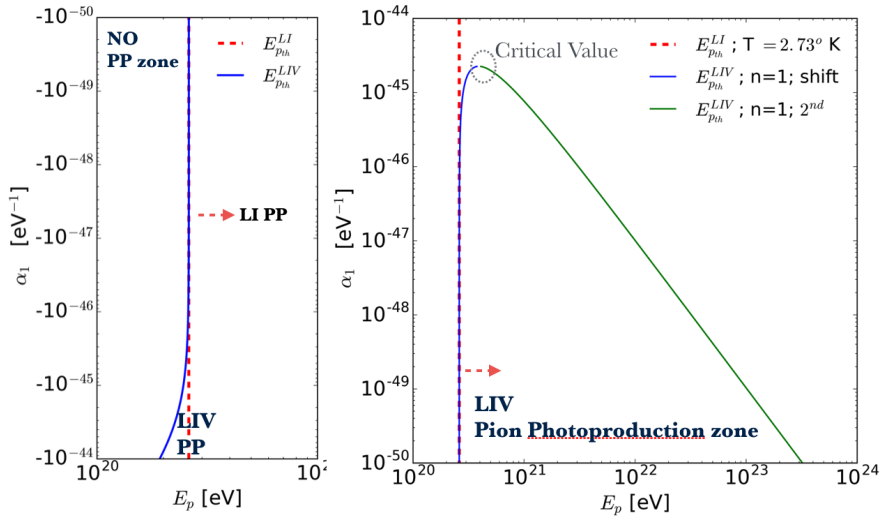

FIGURE 5.3: Threshold shifts by LIV in the photon sector for pion photoproduction. In the left, $\alpha_1 < 0$ while $\alpha_1 > 0$ is in the right.

For example, to illustrate the effects of LIV's shifts, we have chosen the pion photoproduction process by the interaction of a UHECR proton with a CMB-photon. Additionally, let be $\alpha_{p,1} = \alpha_{\pi,1} = 0$, that is, LIV only affects the photon sector. The results can be appreciated in Fig. 5.3. In the left, $\alpha_1 < 0$ while $\alpha_1 < 0$ is in the right. In both figures, the red dotted line is the projection of the LI threshold ($\alpha_1 = 0$). The continued blue line in the left is the solution to the LIV-threshold equation (5.21), and the difference indicates the shift threshold energy to lower energy values. In the right, the two real solutions for the threshold equations are shown, both converge to the critical value, $\alpha_1 = 1.67 \times 10^{-45}\ eV^{-1}$. Above this value, primary cosmic protons would avoid pion photoproduction, and hence the GZK threshold [40, 46, 47]. A small threshold energy shift to higher energies can be appreciated for values close to this critical value. A potential smoothing of the effect is possible once the specifics of flux injection and energy distribution of the photon background be taken into account to calculate the expected cosmic ray fluxes. Nevertheless, we believe this deserves further consideration since it may serve to probe the LIV generic approach's limits.

Chapter 6

Conclusions and remarks

6.1 Conclusions

In the present thesis, we have shown that generic LIV, expressed as the deformation of particle dispersion relations by energy or momentum dependent functions, can be used to study the possible LIV physics without relying on specific models, and thus, more directly and simply.

To demonstrate this, we have addressed three different physical processes relevant in the study of the propagation to the very to ultra high energy cosmic and gamma rays: **vacuum Cherenkov radiation photon decay** and **photoproduction processes**.

The first process, vacuum Cherenkov radiation, was used to validate the generic approximation. We have elaborated a calculation for the emission rate, which considers the standard amplitudes derived from QED rules, but explicitly incorporating the LIV modification of the photon dispersion relation to order n in the photon momentum. All LIV effects for fermions were neglected, though, to be able to compare the results to those of models based on the spontaneous breaking of Lorentz Invariance. The analysis shows that the emission rate does present the same qualitative behavior as the outcomes obtained from the modified Maxwell Theory and the Maxwell-Chern-Simons theory: emission rate grows with the charged particle energy and becomes smaller as α_n does, However, it presents a drop ending threshold which is inversely dependent on the LIV coefficient. This threshold sets the energy value below which LI physics is recovered. We have also analyzed the mass and charge composition sensitivity of the emission rate, and our results show an explicit dependency on the cosmic primary mass and charge, having a more substantial emission rate for heavier nuclei, but with a similar slope and a higher energy threshold. Similar results are found when the modified Maxwell Theory

is used for the calculations. Additionally, we have shown that LIV can motivate a trend to lighter particles in the UHECR cosmic ray spectrum since the vacuum Cherenkov radiation threshold changes with the primary cosmic ray mass and charge.

In the second process, we have implemented the LIV generic approach to photon decay in a vacuum. We have found that photons of sufficient energy are untestable, and once the decay is allowed, the rate is very efficient; last is stringent for the propagation of the cosmic ray primary photons. Nevertheless, as we have argued in this thesis, phase space for outgoing fermions vanishes when photon energy is below critical threshold energy, defined through the expression

$$E_{QG}^{(n)} > k[(k^2 - 4m^2)/4m^2]^{1/n}.$$

The total decay rate becomes zero at such energies, and the process is prohibited, so recovering the standard LI results. Above this threshold, on the other hand, the photon decay rate quickly becomes very large. Thus, the process strongly restricts the possible propagation of the photon to very short distances from the source, to the extent that it becomes unlikely for a primary photon to travel astronomical distances. The aftermath of this is a novel, direct, and straightforward way to bound the LIV energy scale, $E_{QG}^{(n)}$, through the direct observation of the very high energy photons. Using reported gamma telescopes data and photon decay into electron-positron pairs, we have established, for $n = 1$, the stringent bound for the LIV scale at $E_{QG} > 1.5 \times 10^{20}\ GeV$, coming from HEGRA most energetic events.

Finally, generic LIV effects incorporated to all particles involved in the most general photoproduction process, where a high energy cosmic particle interacts with the photon background, producing two particles in the final state, had been shown to modify the LI production threshold. Interestingly enough, our analysis shows that LIV effects are completely general, at first approximation. They do not depend on the particular nature of the particles involved in the process; neither depend on possible linear corrections to energy-momentum conservation. Regardless of the specific photoproduction process, LIV shifts the production threshold towards lower or higher energies. This solely depends on the sign of the overall LIV parametric function, Λ_n, that encodes LIV effects and which enters in a polynomial like the term of order $n+1$ that corrects the, formerly linear, threshold equation. Furthermore, as we have argued, these changes imply an upper bound for the LIV parameter, at $\Lambda_n < (n+1)^{n+1}/(n+2)^{n+2}$. For larger values of Λ_n, photoproduction remains forbidden. Consequently, the shifting on the LIV production threshold is predicted to be always smaller by a factor of $(n+2)/(n+1)$ for $\Lambda_n > 0$. Even more importantly, our analysis has uncovered a novel signature for the LIV physics of photoproduction processes that is worth to underline. Derived from the LIV modification

to the universal threshold equation, a secondary threshold at higher energies will always appear, for $\Lambda_n > 0$, where particle production becomes again forbidden. Above such threshold, cosmic particles shall again propagate freely, giving rise to a possible recovery on the cosmic ray flux.

6.2 Further work

LIV Cherenkov thresholds. As we have discussed in this thesis, this process shows a clear dependency on the cosmic primary mass and charge. Passing the proton emission threshold, protons will be attenuated along with propagation, and the heaviest mass cosmic ray component would become dominant. As energy passes the threshold for heaviest masses, the cosmic rays flux should move again towards the lighter component mass, as a stronger attenuation of heavy particles appears. A detailed calculation of this that considers the astrophysical models for particle injection is needed to understand better the extension of the ultra high energy cosmic rays' effect.

More stringent limits to E_{QG}. The results derived in this thesis for LIV photon decay are a direct and straightforward way to bound LIV energy scale by the single observation of cosmic-ray photons. The new and next generations of gamma-ray telescopes would be able to set new and better limits. The High Altitude Water Cherenkov (HAWC) is sensitive to gamma-rays in the 100 GeV to 100 TeV energy range. The Cherenkov Telescope Array (CTA) is the next-generation ground-based observatory for gamma-ray astronomy at very-high energies. CTA promises to be the world's largest and most sensitive high-energy gamma-ray observatory. The observation of a 100 TeV photon on such observatories may put a bound on $E^{(1)}_{QG}$ of the order of 1×10^{21} GeV.

Photoproduction thresholds. The physical implications of the purely LIV secondary threshold are interesting. A cosmic particle primary shall encounter an opaque Universe along with its propagation, due to photon background, only for primary energies within the two thresholds. At such energies, photoproduction will attenuate the particle's energy, moving it to lower values where the process is switched off, permitting further free propagation. Of course, this is generally the standard LI scenario, but for the shifting of the threshold's actual position. On the other hand, if astrophysical sources injected particle primaries at energies well above the LIV secondary threshold, they would not suffer attenuation due to photoproduction. Recovery on the cosmic particle's primary flux would be expected as a consequence (above the opacity band defined by the thresholds). However, for a complete analysis of the processes arbitrary angle emission has to be considered, as well as the details of the injected primary flux and the photon background energy distribution. Besides, the second threshold happens at very high

energies, and few astrophysical sources are known to produce cosmic ray primaries at such regimes. Even if they do so, candidates are always far enough as to make cosmic expansion effects to be relevant. Redshift diminishes by itself the energy of propagating particles, which means that even if a charged particle primary is produced at high enough energies at source reference frame, local interactions with photon background, on our observer reference frame, would be happening at lower energies. On our frame, at some critical distance between source and observer, the cosmic primary might reach energies where the local Universe becomes again opaque, and energy attenuation would take place as usual. This may still have, however, distinctive features. It shall effectively move the second threshold effects towards an apparently higher energy source, whereas it would move the first threshold closer to the LI value. However, it could also modify the injected flux in the distance to source dependant way, that, if enough data were available, could be distinguishable on the features of the observed flux. A comparison among a set of well-known sources located at different redshifts may serve as a probe to establish observational bounds for the LIV parameters. We believe that these possibilities deserve further study.

6.3 Academical products

The present work have produced the following publications:

- *Restrictions from Lorentz invariance violation on cosmic ray propagation*,
  H. Martínez-Huerta, A. Pérez-Lorenzana.
  Phys. Rev. D 95, 063001 (2017)

- *Effects of Lorentz invariance violation on cosmic ray photon emission and gamma ray decay processes.*
  H. Martínez-Huerta, A. Pérez-Lorenzana.
  PoS (ICRC2017) 556. Presented at the 35th International Cosmic Ray Conference (ICRC2017), Bexco, Busan, Korea. arXiv 1709.08247 [astro-ph.HE]

- *Photon emission and decay from generic Lorentz Invariance Violation.*
  H. Martínez-Huerta, A. Pérez-Lorenzana.
  J. Phys. Conf. Ser., 866 (2016) no. 1, 012006.

- *Vacuum Cherenkov radiation and photon decay rates from generic Lorentz Invariance Violation*,
  H. Martínez-Huerta, A. Pérez-Lorenzana.
  J. Phys. Conf. Ser. 761 (2016) no.1, 012035.

- *Lorentz Invariance Violation on UHECR propagation*,
  H Martínez and A Pérez-Lorenzana.
  J. Phys. Conf. Ser, 468 (2013).

Other publications derived from the results presented in this thesis:

- *Limits on the Lorentz Invariance Violation from UHECR astrophysics*,
  Rodrigo Guedes Lang, Humberto Martínez-Huerta and Vitor de Souza.
  Astrophys.J. 853 (2018) no.1, 23. arXiv 1701.04865

- *Potential constrains on Lorentz invariance violation from the HAWC TeV gamma-rays* .
  H. Martínez et al (HAWC Collaboration).
  HAWC-ICRC-2017-35. PoS (ICRC2017) 868.
  Presented at the 35th International Cosmic Ray Conference (ICRC2017), Bexco, Busan, Korea. arXiv 1708.03384 [astro-ph.HE].

Appendix A

The standard model

The standard model of particles (SM) is a relativistic QFT theory concerning the electromagnetic, weak, and strong interactions [1]. The discoveries of the top quark in 1995, the ν_τ in 2000, and the recent discovery of the Higgs boson in 2012 have given further support to the SM. However, there is plenty of experimental confirmation of the SM. For a review of current measurements and theory of particle physics, see Refs. [76]. In the standard model, there are 12 elementary particles of spin 1/2 (and its antiparticles), known as fermions, 12 bosons of spin 1, and one boson of spin 0. Each particle is an irreducible representation of the Poincare group and is described in terms of a dynamical field on Minkowski space-time.

The gauge symmetry of the SM is SU(3)×SU(2)×U(1). The SU(3) component correspond to colored quarks and gluons' interactions described by quantum chromodynamics (QCD). On the other hand, the standard model of electroweak interactions (EW) is based on the SU(2)×U(1) group.

The latter includes the gauge bosons W^i_μ and B_μ, with $i = 1, 2, 3$, for the SU(2) and U(1), respectively. As usual, the corresponding gauge coupling constants will be named g and g', hereafter. Under SU(2), the left-handed fermion fields transform as doublets; thus, let them be

$$(\Psi_i)_L = \begin{pmatrix} \nu_i \\ l_i^- \end{pmatrix} \quad \text{and} \quad \begin{pmatrix} u_i \\ d'_i \end{pmatrix}, \tag{A.1}$$

where $d'_i = \sum_j V_{ij} d_j$ and V is the Cabibbo-Kobayashi-Maskawa mixing matrix that can be parametrized by three mixing angles, θ_{ij} and a CP-violation phase, δ. The index i stands for the i-th fermion family; there are only three of them in the minimal standard model. CP-violating is incorporated into the EW model by a single observable phase

[1] The present appendix was mainly made following the summaries presented in Ref. [76]. For more details, the reader could refer to it and its references.

V_{ij}. An extension of the formalism can be made to include neutrino masses, mixings, and oscillations.

The right-handed fermion fields are singlets under $SU(2)$ and can be written as

$$(\psi_i)_R = (l_i^-)_R \ , \quad (u_i)_R \ , \quad \text{and} \quad (d_i)_R. \tag{A.2}$$

where ψ_i denotes the fermion field.

A complex scalar Higgs doublet generates the elementary particle masses in the SM,

$$\phi = \begin{pmatrix} \phi^+ \\ \phi^0 \end{pmatrix}, \tag{A.3}$$

through spontaneous symmetry breaking of the potential given by

$$\mathcal{V}(\Phi) = \mu^2 \phi^\dagger \phi + \frac{\lambda^2}{2} (\phi^\dagger \phi)^2. \tag{A.4}$$

If $\mu^2 < 0$, ϕ develops a vacuum expectation value (VEV), $v = \sqrt{2}\frac{\mu}{\lambda} = (\sqrt{2} G_F)^{-1/2} \sim$ 246 GeV.

After the breaking of the EW gauge symmetry, only a neutral Higgs scalar remains in the physical particle spectrum. Consequently the Lagrangian for the fermion fields, ψ_i, can be written as

$$\begin{aligned} \mathcal{L}_\mathcal{F} = & \sum_i \bar{\psi}_i \left(i\partial\!\!\!/ - m_i - \frac{m_i H}{v} \right) \psi_i \\ & - \frac{g}{2\sqrt{2}} \sum_i \bar{\Psi}_i \gamma^\mu (1 - \gamma^5)(T^+ W_\mu^+ + T^- W_\mu^-) \Psi_i \\ & - \frac{g}{2 \cos\theta_W} \sum_i \bar{\psi}_i \gamma^\mu (g_V^i - g_A^i \gamma^5) \psi_i Z_\mu \\ & - e \sum_i Q_i \bar{\psi}_i \gamma_\mu \psi_i A_\mu, \end{aligned} \tag{A.5}$$

where[2]

γ^μ,	are the Dirac γ-matrices;
$\theta_W = \tan^{-1}(g'/g)$,	is the weak angle;
$e = g \sin\theta_W$,	is the positron electric charge, which leads to $\alpha_{EW} = e^2/4\pi$, the fine-structure constant;
T^+ and T^-,	are the weak isospin raising and lowering operators;
Q_i,	is the charge of ψ_i in e units;

[2]Natural units are assumed $\hbar = c = \epsilon_0 = 1$ and Minkowski metric (1,-1,-1,-1).

$A = B\cos\theta_W + W^3\sin\theta_W$,	is the photon field;
$W^\pm = (W^1 \pm iW^2)/\sqrt{2}$,	is the charged weak boson field;
$Z = B\sin\theta_W + W^3$,	is the neutral weak boson field;
$g\dfrac{m_i}{2M_W}$,	is the Yukawa coupling of H to ψ_i, which in the minimal model is diagonal;
$g_V^i = t_{3L}(i) - 2Q_i\sin^2\theta_W$,	is the vector coupling;
$g_A^i = t_{3L}(i)$,	is the axial coupling;
$t_{3L}(i) = Q_i - \dfrac{1}{2}Y_i$,	is the weak isospin of i-th fermion;
Y_i,	is the hypercharge of i-th fermion.

Additionally, at the lowest order in perturbation theory, i.e., at tree level, the boson masses in the EW sector are given by

$$\begin{aligned} M_H &= \lambda v, \quad M_W = \frac{1}{2}gv = \frac{ev}{2\sin\theta_W}, \quad M_\gamma = 0, \\ M_Z &= \frac{1}{2}\sqrt{g^2+g'^2}v = \frac{ev}{2\sin\theta_W\cos\theta_W} = \frac{M_W}{\cos\theta_W}. \end{aligned} \tag{A.6}$$

The first term in Eq. (A.5) corresponds to the kinematic and mass fermion terms. In the presence of right-handed neutrinos, it gives rise to Dirac neutrino masses. The second term represents the charged-current weak interaction, which for the coupling of a $W^\pm$ to an electron and a neutrino gives

$$\mathcal{L}_{cc}^{(W^\pm\ l_e)} = \frac{e}{2\sqrt{2}\sin\theta_W}\left[W_\mu^-\bar{l}_e\gamma^\mu(1-\gamma^5)\nu_e + W_\mu^+\bar{\nu_e}\gamma^\mu(1-\gamma^5)l_e)\right]. \tag{A.7}$$

A similar expression can be written for quarks. In the limit for small momenta compared to M_W, the last expression produces the effective four-fermion interaction after the identification of the Fermi constant,

$$G_F = \frac{\sqrt{2}g^2}{8M_W^2} = \frac{1}{\sqrt{2}v^2} = 1.1663787(6)\times 10^{-5}\text{GeV}^{-2}. \tag{A.8}$$

Last argument can be seen by considering for instance $\nu_\mu\ e \to \nu_e\ \mu$.

The third term in Eq. (A.5) is the weak neutral-current interaction, which includes the weak isospin of fermions, $t_{3L}(i)$. In table A.1 we show the charge (Q_i), hypercharge (Y_i), and isospin values for leptons and quarks in the minimal standard model, where the hypercharge is the generator of $U(1)$ and satisfies the relation $Y_i = 2(Q_i - t_{3L}(i))$. Finally, the last term describes electromagnetic interactions, or quantum electrodynamics theory (QED).

In Appendix B, an additional notation is used to separate out the different sectors of the SM, which includes a classification of fermions in lepton and quark terms to clarify

	Chirality	Fields	SU(2)	Q	Y	t_{3L}
Leptons	left-handed	$\begin{pmatrix} \nu_i \\ l_i^- \end{pmatrix}$	doublet	0 -1	-1 -1	$1/2$ $-1/2$
	right-handed	$(l_i^-)_R$	singlet	-1	-2	0
Quarks	left-handed	$\begin{pmatrix} u_i \\ d_i \end{pmatrix}$	doublet	$2/3$ $-1/3$	$1/3$ $1/3$	$1/2$ $-1/2$
	right-handed	u_R d_R	singlet	$2/3$ $-1/3$	$4/3$ $-2/3$	0 0

TABLE A.1: Charge (Q), hypercharge (Y) and isospin (t_{3L}) values for leptons and quarks in the minimal standard model.

the contributions from the spontaneous Lorentz symmetry breaking in the mSME.

Additionally to fermions in EW theory, in QCD, quarks are in the fundamental representation of SU(3) color group, so let be $\psi_{q,a}$ a quark-field spinor for a quark of flavor q, mass m_q and color index a. However, since quarks have 3-colors, the color index runs from $a = 1$ to $N_C = 3$. Additionally, eight kinds of gluons have to be included; thus, let be A_μ^C the gluon fields, with C running from 1 to $N_C^2 - 1 = 8$, where gluons transform in the adjoint representation of SU(3) color group. Hence, the Lagrangian of QCD is given by

$$\mathcal{L}_{\mathcal{QCD}} = \sum_q \bar{\psi}_{q,a}(i\gamma^\mu \partial_\mu \delta_{a,b} - g_s \gamma^\mu t_{ab}^C A_\mu^C - m_q \delta_{ab})\psi_{q,b} - \frac{1}{4} F_{\mu\nu}^A F^{A\mu\nu}, \tag{A.9}$$

where $t_{a,b}^C$ correspond to the eight generators of SU(3), which are 3×3 matrices. g_s is the coupling constant in QCD and the field-strength tensor $F_{\mu\nu}^A F^{A\mu\nu}$ is given by

$$F_{\mu\nu}^A = \partial_\mu A_\nu^A - \partial_\nu A_\mu^A - g_s f_{ABC} A_\mu^B A_\nu^C, \tag{A.10}$$

where the structure constants of SU(3), f_{ABC}, satisfy $[t^A, t^B] = i f_{ABC}$. The fundamental parameters of QCD are the quark masses and the coupling constant, g_s, that can be expressed as

$$\alpha_s = \frac{g_s^2}{4\pi}. \tag{A.11}$$

Worth to mention that, although there are three different colors for quarks and gluons, hadrons are colorless, i.e., color-singlet.

There is a freedom for an additional CP-violating term in the $\mathcal{L}_{\mathcal{QCD}}$, and is given by

$$\mathcal{L}_{QCD}^{CP-v} = \theta_{QCD} \frac{\alpha_s}{8\pi} F_{\mu\nu}^A \widetilde{F}^{\ A\mu\nu}, \tag{A.12}$$

with $\widetilde{F}_{\mu\nu}^A = 1/2\epsilon_{\mu\nu\sigma\rho} F^{A\sigma\rho}$, the dual of the gluon field tensor. However, stringent limits have been set to this parameter. Notice that additionally to θ_{QCD}, there are also 18 free

parameters, which values are experimentally given to the theory and are summarized in Tab. A.2.

	Parameter	**Experimental value**
m_e,	electron mass	$0.510998928 \pm 0.000000011$ MeV
m_μ,	muon mass	$105.6583715 \pm 0.0000035$ MeV
m_τ,	tau mass	1776.82 ± 0.16 MeV
m_u,	up quark mass	$2.3^{+0.7}_{-0.5}$ MeV
m_d,	down quark mass	$4.8^{+0.5}_{-0.3}$ MeV
m_s,	strange quark mass	95 ± 5 MeV
m_c,	charm quark mass	1.275 ± 0.025 GeV
m_b,	bottom quark mass	4.18 ± 0.03 GeV
m_t,	top quark mass	173.2 ± 0.9 GeV
v,	Higgs VEV	246 GeV
m_H,	Higgs mass	125.7 ± 0.4 GeV
θ_{12},	CKM 12-mixing angle	13.04 ± 0.05^o
θ_{23},	CKM 23-mixing angle	0.201 ± 0.011^o
θ_{13},	CKM 13-mixing angle	2.38 ± 0.06^o
δ,	CKM CP-violating phase	1.20 ± 0.08^o
$\sin^2\theta_W$,	weak angle	0.23129(5)
α_{EW},	fine structure constant	1/137.035999074(44)
$\alpha_s(M_z^2)$,	SU(3) gauge coupling	0.1185 ± 0.0006
$\lvert\theta_{QCD}\rvert$,	QCD vacuum angle	$\lesssim 10^{-11}$

TABLE A.2: Free parameters in the mSM and their experimental values reported in Ref. [76]

Appendix B

The mSME

In the present appendix, we introduce the minimal Lorentz-violating extension of the standard model (mSME) as it was presented and developed by Collady and Kostelecky in their 1998 work [11].

The mSME adds to the standard model all possible coordinate-invariant operators formed by combining SM and gravitational fields. These possible Lorentz-violating terms are only those that could arise from spontaneous breaking of Lorentz symmetry at the fundamental level, but that preserves $SU(3) \times SU(2) \times U(1)$ gauge invariance and power-counting renormalizability.

Spontaneous Lorentz symmetry breaking may occur in nonlinear gauge electrodynamics [1], in the context of string theories with Lorentz-covariant dynamics [34], or also in a framework developed for treating the effects of spontaneous Lorentz breaking in the context of low energy effective theory [77], among others.

Due to the spontaneous breaking of Lorentz symmetry, LI remains property of the underlying fundamental theory, so micro-causality and positivity of the energy are expected to hold in the low-energy effective theory. Energy and momentum are conserved as usual. Also, the standard quantization methods are unaffected. Hence the relativistic Dirac equation and the non-relativistic Schrodinger equation emerge in the appropriate limits.

Since the fundamental theory and the effective low-energy theory are invariant under observer Lorentz transformation, they are invariant under rotations or boost of an observer's inertial frame. However, the nonzero tensor expectation values in vacuum affect only invariance properties under particle Lorentz transformations, that is, rotations or boost of localized field particles that leave unchanged the background expectation values.

Two types of coefficients arise from the general Lorentz-violating terms. Those that act as coupling coefficients and those constructed from the basic fields in the standard

model. The first type carries space-time indices and reflects the properties under observer Lorentz transformations of the fundamental theory's nonzero expectation values. The coupling coefficient may be complex, but the requirement of Lagrangian Hermiticity constrains it. Additionally, for coefficients of this type with an even number of space-time indices, the pure trace component is irrelevant since it maintains Lorentz invariance, and it can be taken traceless. The second type, the field coefficients, involve covariant derivatives, and γ matrices for those that involve fermions. They are singlets under $SU(3) \times SU(2) \times U(1)$ gauge invariance and must have mass dimension no greater than four due to power-counting renormalizability. Additionally, since the SME originates from spontaneous Lorentz breaking in a covariant fundamental theory, the field terms must be a singlet under observer Lorentz transformations. Hence they must have indices matching those of the coupling coefficient. A summary of the main and general properties of the coefficients is presented in Tab. B.1 at the end of this section.

All coupling coefficients are assumed to be heavily suppressed by some power of the ratio among light scale to the Plank scale, and a term with mass dimension n must have a coupling coefficient with a mass dimension $4 - n$. Several constraints have been made so far by different techniques. For the complete list of constraints and limits of the SME see Ref. [39].

In the following lines, all renormalizable terms compatible with the gauge symmetries of the standard model and with an origin in spontaneous Lorentz breaking are presented[1].

Let be the left and right-handed lepton and quark multiplets

$$L_A = \begin{pmatrix} \nu_A \\ l_A \end{pmatrix}, \quad R_A = (l_A)_R,$$

$$Q_A = \begin{pmatrix} u_A \\ d_A \end{pmatrix}, \quad U_A = (u_A)_R, \quad D_A = (d_A)_R,$$

where $A = 1, 2, 3$ labels the flavor:

$$l_A = (e, \mu, \tau), \quad \nu_A = (\nu_e, \nu_\mu, \nu_\tau),$$

$$u_A = (u, c, t) \quad \text{and} \quad d_A = (d, s, b).$$

Additionally, let the Higgs doublet in a unitary gauge be

$$\phi = \frac{1}{\sqrt{2}} \begin{pmatrix} 0 \\ r_\phi \end{pmatrix},$$

[1] Natural units are assumed $\hbar = c = \epsilon_0 = 1$ and Minkowski metric (1,-1,-1,-1).

and be the Gauge fields G_μ, W_μ and B_μ, with the corresponding field strengths $G_{\mu\nu}$ and $W_{\mu\nu}$, Hermitian adjoint matrices, and $B_{\mu\nu}$ a Hermitian singlet. Also, let be the corresponding couplings g_3, g and g', whereas q stand for the electromagnetic charge U(1), that satisfies $q = g\sin\theta_W = g'\cos\theta_W$. As usual, we denote the covariant derivative as D_μ and $A\overleftrightarrow{\partial}_\mu B = A\partial_\mu B - (\partial_\mu A)B$. Also, let be the Yukawa couplings denoted as G_L, G_u and G_D.

Separating out the new contributions into the SU(3)×SU(2)×U(1) SM sectors and by $CPT-even$ and $CPT-odd$ parts, the Lagrangian terms are as follows.

For the lepton sector,

$$\mathcal{L}_{lepton} = \frac{1}{2}i\bar{L}_A\gamma^\mu\overleftrightarrow{D}_\mu L_B + \frac{1}{2}i\bar{R}_A\gamma^\mu\overleftrightarrow{D}_\mu R_B, \tag{B.1}$$

$$\mathcal{L}^{CPT-even}_{lepton} = \frac{1}{2}i(c_L)_{\mu\nu AB}\bar{L}_A\gamma^\mu\overleftrightarrow{D}_\mu L_B + \frac{1}{2}i(c_R)_{\mu\nu AB}\bar{R}_A\gamma^\mu\overleftrightarrow{D}_\mu R_B, \tag{B.2}$$

$$\mathcal{L}^{CPT-odd}_{lepton} = -(a_L)_{\mu AB}\bar{L}_A\gamma^\mu L_B + (a_R)_{\mu AB}\bar{R}_A\gamma^\mu R_B. \tag{B.3}$$

For the quark sector,

$$\mathcal{L}^{CPT-even}_{quark} = \frac{1}{2}i\bar{Q}_A\gamma^\mu\overleftrightarrow{D}_\mu Q_B + \frac{1}{2}i\bar{U}_A\gamma^\mu\overleftrightarrow{D}_\mu U_B + \frac{1}{2}i\bar{D}_A\gamma^\mu\overleftrightarrow{D}_\mu D_B, \tag{B.4}$$

$$\begin{aligned}\mathcal{L}^{CPT-even}_{quark} =& \frac{1}{2}i(c_Q)_{\mu\nu AB}\bar{Q}_A\gamma^\mu\overleftrightarrow{D}_\mu Q_B \\ &+ \frac{1}{2}i(c_U)_{\mu\nu AB}\bar{U}_A\gamma^\mu\overleftrightarrow{D}_\mu U_B + \frac{1}{2}i(c_D)_{\mu\nu AB}\bar{D}_A\gamma^\mu\overleftrightarrow{D}_\mu D_B,\end{aligned} \tag{B.5}$$

$$\mathcal{L}^{CPT-odd}_{quark} = -(a_Q)_{\mu AB}\bar{Q}_A\gamma^\mu Q_B - (a_U)_{\mu AB}\bar{U}_A\gamma^\mu U_B - (a_D)_{\mu AB}\bar{D}_A\gamma^\mu D_B. \tag{B.6}$$

For the Yukawa sector,

$$\begin{aligned}\mathcal{L}_{Yukawa} =& -\frac{1}{2}[(G_L)_{AB}\bar{L}_A\phi\gamma^\mu R_B \\ &+ \frac{1}{2}(G_U)_{AB}\bar{Q}_A\phi\gamma^\mu U_B + \frac{1}{2}(G_D)_{AB}\bar{Q}_A\phi\gamma^\mu D_B] + h.c.,\end{aligned} \tag{B.7}$$

$$\begin{aligned}\mathcal{L}^{CPT-even}_{Yukawa} =& -\frac{1}{2}[(H_L)_{\mu\nu AB}\bar{L}_A\phi\gamma^\mu\sigma^{\mu\nu}R_B \\ &+ \frac{1}{2}(H_U)_{\mu\nu AB}\bar{Q}_A\phi\gamma^\mu\sigma^{\mu\nu}U_B + \frac{1}{2}(H_D)_{\mu\nu AB}\bar{Q}_A\phi\gamma^\mu\sigma^{\mu\nu}D_B] + h.c.\end{aligned} \tag{B.8}$$

For the Higgs sector,

$$\mathcal{L}_{Higgs} = (D_\mu\phi)^\dagger D^\mu\phi + \mu^2\phi^\dagger\phi - \frac{\lambda}{3!}(\phi^\dagger\phi)^2, \tag{B.9}$$

$$\begin{aligned}\mathcal{L}_{Higgs}^{CPT-even} =& \frac{1}{2}(k_{\phi\phi})^{\mu\nu}(D_\mu\phi)^\dagger D_\nu\phi + h.c. \\ &- \frac{1}{2}(k_{\phi B})^{\mu\nu}\phi^\dagger\phi B_{\mu\nu} - \frac{1}{2}(k_{\phi W})^{\mu\nu}\phi^\dagger W_{\mu\nu}\phi\end{aligned} \tag{B.10}$$

$$\mathcal{L}_{Higgs}^{CPT-odd} = i(k_\phi)^\mu\phi^\dagger D_\mu\phi + h.c. \tag{B.11}$$

And for the gauge sector,

$$\mathcal{L}_{gauge} = -\frac{1}{2}\mathrm{Tr}(\mathrm{G}_{\mu\nu}\mathrm{G}^{\mu\nu}) - \frac{1}{2}\mathrm{Tr}(\mathrm{W}_{\mu\nu}\mathrm{W}^{\mu\nu}) - \frac{1}{4}\mathrm{B}_{\mu\nu}\mathrm{B}^{\mu\nu}, \tag{B.12}$$

$$\begin{aligned}\mathcal{L}_{gauge}^{CPT-even} =& -\frac{1}{2}(k_G)^{\kappa\lambda\mu\nu}\mathrm{Tr}(\mathrm{G}^{\kappa\lambda}\mathrm{G}^{\mu\nu}) \\ &- \frac{1}{2}(k_W)^{\kappa\lambda\mu\nu}\mathrm{Tr}(\mathrm{W}^{\kappa\lambda}\mathrm{W}^{\mu\nu}) - \frac{1}{4}(\mathrm{k_B})^{\kappa\lambda\mu\nu}\mathrm{B}^{\kappa\lambda}\mathrm{B}^{\mu\nu},\end{aligned} \tag{B.13}$$

$$\begin{aligned}\mathcal{L}_{gauge}^{CPT-odd} =& (k_3)_\kappa\epsilon^{\kappa\lambda\mu\nu}\mathrm{Tr}(\mathrm{G}_\lambda\mathrm{G}_{\mu\nu} + \frac{2}{3}\mathrm{ig_3G}_\lambda\mathrm{G}_\mu\mathrm{G}_\nu) \\ &+ (k_2)_\kappa\epsilon^{\kappa\lambda\mu\nu}\mathrm{Tr}(\mathrm{W}_\lambda\mathrm{W}_{\mu\nu} + \frac{2}{3}\mathrm{igW}_\lambda\mathrm{W}_\mu\mathrm{W}_\nu) \\ &+ (k_1)_\kappa\epsilon\kappa\lambda\mu\nu B^\lambda B_{\mu\nu} + (k_0)_\kappa B^\kappa.\end{aligned} \tag{B.14}$$

The θ terms and possible analogous total-derivative terms that break Lorentz symmetry are omitted.

Sector	Coefficient	Mass Dim.	Notes
Fermion	$c_{\mu\nu}$	0	Hermitian in generation space
Fermion	a_μ	1	Hermitian in generation space. Symmetric and antisymmetric but traceless[2].
Yukawa	$H_{\mu\nu}$	0	Antisymmetric. Not necessarily Hermitian in generation space.
Higgs	$k_{\phi\phi}$	0	Can have symmetric real and antisymmetric imaginary parts.
Higgs	$k_{\phi B}, k_{\phi W}$	1	Must be real and antisymmetric.
Higgs	k_ϕ	1	Can be an arbitrary complex number.
Gauge	$k_{G,W,B}$	0	Real. Must have the symmetries of the Riemann tensor and vanishing double trace.[3]
Gauge	$k_{1,2,3}$	1	Real.
Gauge	k_0	3	Real[4].

TABLE B.1: Remarks on mSME coefficients.

B.1 The Pure-photon sector

In the present thesis, the mSME sector of interest is the $U(1)$ gauge-invariant pure-photon sector, where

$$\mathcal{L}_{photon} = -\frac{1}{4}F_{\mu\nu}F^{\mu\nu}, \tag{B.15}$$

$$\mathcal{L}_{photon}^{CPT-even} = -\frac{1}{4}(k_F)_{\kappa\lambda\mu\nu}F^{\kappa\lambda}F^{\mu\nu}, \tag{B.16}$$

$$\mathcal{L}_{photon}^{CPT-odd} = +\frac{1}{2}(k_{AF})^\kappa \epsilon_{\kappa\lambda\mu\nu}A^\lambda F^{\mu\nu}. \tag{B.17}$$

The couplings $(k_F)_{\kappa\lambda\mu\nu}$ arise from $\mathcal{L}_{gauge}^{CPT-even}$ in Eq. (B.13). And similarly to $k_{G,W,B}$, they are real and dimensionless and can be taken to have the symmetries of the Riemann tensor. Similarly, $(k_{AF})^\kappa$ arises from $\mathcal{L}_{gauge}^{CPT-odd}$ in Eq. (B.14) and it is real and has mass dimensions one.

The coupling $(k_F)_{\kappa\lambda\mu\nu}$ can be taken as double traceless,

$$k^{\mu\nu}{}_{\mu\nu} = 0, \tag{B.18}$$

[2] A nonzero trace would not contribute to Lorentz violation and can be absorbed by a conventional field normalization.

[3] Any totally antisymetric part involves only a total derivative in the $\mathcal{L}$, while a nonzero double trace can be absorbed into a redefinition of the normalization of the corresponding kinetic term $\mathcal{L}_{gauge}$.

[4] Is desirable that all the coefficients $k_{0,1,2,3}$ vanish since they should generate instabilities in the minimal theory.

since any trace component can be renamed through simple field redefinition in the kinetic term $\mathcal{L}_{photon}$, such that, it just leads to a field renormalization.

For certain calculations, like the ones presented in this thesis and in Ref. [11, 35], it is certainly useful to decompose the coefficient k_f into its two Lorentz-irreducible parts, one with ten independent components as the Weyl tensor in GR and the other with nine components analogous to the trace-free Ricci tensor. It is also demanded to obey the same symmetries which hold for the Riemann curvature tensor,

$$k_{\mu\nu\rho\lambda} = -k_{\nu\mu\rho\lambda} = k_{\nu\mu\lambda\rho}, \quad k_{\mu\nu\rho\lambda} = k_{\rho\lambda\mu\nu}, \tag{B.19}$$

such that, only 19 total independent components remain. Moreover, only the (00) component of the trace-free Rici-tensor analog is associated with the invariant terms under particle rotations.

Similarly, only one of the four independent components of the coefficient k_{AF}, the time-like component, k^0_{AF}, is associated with the terms under invariant particle rotations.

Bibliography

[1] Yoichiro Nambu. Quantum electrodynamics in nonlinear gauge. *Supplement of the Progress of Theoretical Physics*, Extra Number:190–195, 1968.

[2] Robert Bluhm. Observational Constraints on Local Lorentz Invariance. In Abhay Ashtekar and Vesselin Petkov, editors, *Springer Handbook of Spacetime*, pages 485–507. 2014. doi: 10.1007/978-3-642-41992-8_23. URL `http://inspirehep.net/record/1217717/files/arXiv:1302.1150.pdf`.

[3] Robertus Potting. Lorentz and CPT violation. *J. Phys. Conf. Ser.*, 447:012009, 2013. doi: 10.1088/1742-6596/447/1/012009.

[4] Jorge Alfaro. Quantum gravity and Lorentz invariance deformation in the standard model. *Phys. Rev. Lett.*, 94:221302, 2005. doi: 10.1103/PhysRevLett.94.221302.

[5] Giovanni Amelino-Camelia. A Phenomenological description of quantum gravity induced space-time noise. *Nature*, 410:1065–1067, 2001. doi: 10.1038/35074035.

[6] John R. Ellis, N. E. Mavromatos, and Dimitri V. Nanopoulos. Quantum gravitational diffusion and stochastic fluctuations in the velocity of light. *Gen. Rel. Grav.*, 32:127–144, 2000. doi: 10.1023/A:1001852601248.

[7] John R. Ellis, N. E. Mavromatos, Dimitri V. Nanopoulos, and G. Volkov. Gravitational recoil effects on fermion propagation in space-time foam. *Gen. Rel. Grav.*, 32:1777–1798, 2000. doi: 10.1023/A:1001980530113.

[8] John R. Ellis, N. E. Mavromatos, and Dimitri V. Nanopoulos. A microscopic recoil model for light cone fluctuations in quantum gravity. *Phys. Rev.*, D61: 027503, 2000. doi: 10.1103/PhysRevD.61.027503.

[9] Rodolfo Gambini and Jorge Pullin. Nonstandard optics from quantum space-time. *Phys. Rev.*, D59:124021, 1999. doi: 10.1103/PhysRevD.59.124021.

[10] For alternative models see also: G. Calcagni. Lorentz Violations in Multifractal Spacetimes. 2016.

[11] D. Colladay and V. Alan Kostelecky. Lorentz-violating extension of the standard model. *Phys. Rev. D*, 58:116002, 1998.

[12] Sidney R. Coleman and Sheldon L. Glashow. High-energy tests of Lorentz invariance. *Phys. Rev.*, D59:116008, 1999. doi: 10.1103/PhysRevD.59.116008.

[13] Robert C. Myers and Maxim Pospelov. Ultraviolet modifications of dispersion relations in effective field theory. *Phys. Rev. Lett.*, 90:211601, 2003. doi: 10.1103/PhysRevLett.90.211601.

[14] V. Vasileiou, A. Jacholkowska, F. Piron, J. Bolmont, C. Couturier, J. Granot, F. W. Stecker, J. Cohen-Tanugi, and F. Longo. Constraints on Lorentz Invariance Violation from Fermi-Large Area Telescope Observations of Gamma-Ray Bursts. *Phys. Rev.*, D87(12):122001, 2013. doi: 10.1103/PhysRevD.87.122001.

[15] Giovanni Amelino-Camelia. A Phenomenological description of quantum gravity induced space-time noise. *Nature*, 410:1065–1067, 2001. doi: 10.1038/35074035.

[16] Dharam Vir Ahluwalia. Quantum gravity: Testing time for theories. *Nature*, 398: 199, 1999. doi: 10.1038/18325.

[17] G. Amelino-Camelia, John R. Ellis, N. E. Mavromatos, Dimitri V. Nanopoulos, and Subir Sarkar. Tests of quantum gravity from observations of gamma-ray bursts. *Nature*, 393:763–765, 1998. doi: 10.1038/31647.

[18] T. Jacobson, S. Liberati, and D. Mattingly. Threshold effects and planck scale lorentz violation: Combined constraints from high energy astrophysics. *Phys. Rev. D*, 67:124011, Jun 2003. doi: 10.1103/PhysRevD.67.124011. URL `http://link.aps.org/doi/10.1103/PhysRevD.67.124011`.

[19] Matteo Galaverni and Gunter Sigl. Lorentz Violation in the Photon Sector and Ultra-High Energy Cosmic Rays. *Phys. Rev. Lett.*, 100:021102, 2008. doi: 10.1103/PhysRevLett.100.021102.

[20] Matteo Galaverni and Gunter Sigl. Lorentz Violation and Ultrahigh-Energy Photons. *Phys. Rev.*, D78:063003, 2008. doi: 10.1103/PhysRevD.78.063003.

[21] S. T. Scully and F. W. Stecker. Lorentz Invariance Violation and the Observed Spectrum of Ultrahigh Energy Cosmic Rays. *Astropart. Phys.*, 31:220–225, 2009. doi: 10.1016/j.astropartphys.2009.01.002.

[22] Floyd W. Stecker and Sean T. Scully. Searching for New Physics with Ultrahigh Energy Cosmic Rays. *New J. Phys.*, 11:085003, 2009. doi: 10.1088/1367-2630/11/8/085003.

[23] Sidney R. Coleman and Sheldon L. Glashow. Cosmic ray and neutrino tests of special relativity. *Phys. Lett.*, B405:249–252, 1997. doi: 10.1016/S0370-2693(97)00638-2.

[24] H. Martínez-Huerta and A. Pérez-Lorenzana. Restrictions from Lorentz invariance violation on cosmic ray propagation. *Phys. Rev.*, D95(6):063001, 2017. doi: 10.1103/PhysRevD.95.063001.

[25] Haowei Xu and Bo-Qiang Ma. Light speed variation from gamma ray burst GRB 160509A. *Phys. Lett.*, B760:602–604, 2016. doi: 10.1016/j.physletb.2016.07.044.

[26] Lukas Nellen. The potential of the HAWC Observatory to observe violations of Lorentz Invariance. *PoS*, ICRC2015:850, 2016.

[27] M. Schreck. Obtaining bounds from ultra-high energy cosmic rays in isotropic modified Maxwell theory. In *Proceedings, 6th Meeting on CPT and Lorentz Symmetry (CPT 13): Bloomington, Indiana, USA, June 17-21, 2013*, pages 176–179, 2014. doi: 10.1142/9789814566438_0044. URL `http://inspirehep.net/record/1261431/files/arXiv:1310.5159.pdf`.

[28] Benjamin Zitzer. Lorentz Invariance Violation Limits from the Crab Pulsar using VERITAS. page 1147, 2013. URL `http://inspirehep.net/record/1245458/files/arXiv:1307.8382.pdf`.

[29] A. Nepomuk Otte. Prospects of performing Lorentz invariance tests with VHE emission from pulsars. In *Proceedings, 32nd International Cosmic Ray Conference (ICRC 2011): Beijing, China, August 11-18, 2011*, volume 7, pages 256–259, 2012. doi: 10.7529/ICRC2011/V07/1302. URL `http://inspirehep.net/record/1127202/files/arXiv:1208.2033.pdf`.

[30] A. Abramowski et al. Search for Lorentz Invariance breaking with a likelihood fit of the PKS 2155-304 Flare Data Taken on MJD 53944. *Astropart. Phys.*, 34: 738–747, 2011. doi: 10.1016/j.astropartphys.2011.01.007.

[31] John R. Ellis, Nick E. Mavromatos, Dimitri V. Nanopoulos, Alexander S. Sakharov, and Edward K. G. Sarkisyan. Robust limits on Lorentz violation from gamma-ray bursts. *Astropart. Phys.*, 25:402–411, 2006. doi: 10.1016/j.astropartphys.2006.04.001,10.1016/j.astropartphys.2007.12.003. [Erratum: Astropart. Phys.29,158(2008)].

[32] J. Albert et al. Probing Quantum Gravity using Photons from a flare of the active galactic nucleus Markarian 501 Observed by the MAGIC telescope. *Phys. Lett.*, B668:253–257, 2008. doi: 10.1016/j.physletb.2008.08.053.

[33] John R. Ellis, N. E. Mavromatos, Dimitri V. Nanopoulos, and Alexander S. Sakharov. Quantum-gravity analysis of gamma-ray bursts using wavelets. *Astron. Astrophys.*, 402:409–424, 2003. doi: 10.1051/0004-6361:20030263.

[34] V. Alan Kostelecky and Stuart Samuel. Spontaneous Breaking of Lorentz Symmetry in String Theory. *Phys. Rev.*, D39:683, 1989. doi: 10.1103/PhysRevD.39.683.

[35] F. R. Klinkhamer and M. Schreck. New two-sided bound on the isotropic Lorentz-violating parameter of modified-Maxwell theory. *Phys. Rev.*, D78:085026, 2008. doi: 10.1103/PhysRevD.78.085026.

[36] C. Kaufhold, F. R. Klinkhamer, and M. Schreck. Tree-level calculation of vacuum cherenkov radiation in isotropic nonbirefringent modified-maxwell theory. *KA-TP*, 32:26, 2007.

[37] C. Kaufhold and F. R. Klinkhamer. Vacuum Cherenkov radiation in spacelike Maxwell-Chern-Simons theory. *Phys. Rev.*, D76:025024, 2007. doi: 10.1103/PhysRevD.76.025024.

[38] Sean M. Carroll, George B. Field, and Roman Jackiw. Limits on a Lorentz and Parity Violating Modification of Electrodynamics. *Phys. Rev.*, D41:1231, 1990. doi: 10.1103/PhysRevD.41.1231.

[39] V. Alan Kostelecky and Neil Russell. Data Tables for Lorentz and CPT Violation. *Rev. Mod. Phys.*, 83:11–31, 2011. doi: 10.1103/RevModPhys.83.11.

[40] J. Abraham et al. Measurement of the energy spectrum of cosmic rays above 10^{18} eV using the Pierre Auger Observatory. *Phys. Lett.*, B685:239–246, 2010. doi: 10.1016/j.physletb.2010.02.013.

[41] K. A. Olive et al. Review of Particle Physics. *Chin. Phys.*, C38:090001, 2014. doi: 10.1088/1674-1137/38/9/090001.

[42] Andreas Haungs. Cosmic Rays from the Knee to the Ankle. *Phys. Procedia*, 61: 425–434, 2015. doi: 10.1016/j.phpro.2014.12.094.

[43] A Haungs et al. Investigating the 2nd knee: The kascade-grande experiment. *Journal of Physics: Conference Series*, 47(1):238, 2006. URL `http://stacks.iop.org/1742-6596/47/i=1/a=029`.

[44] S. Schoo et al. KASCADE-Grande Review, Recent Results, Future Endeavors. *JPS Conf. Proc.*, 9:010010, 2016. doi: 10.7566/JPSCP.9.010010.

[45] J. C. Arteaga-Velázquez et al. The KASCADE-Grande observatory and the composition of very high-energy cosmic rays. *J. Phys. Conf. Ser.*, 651(1):012001, 2015. doi: 10.1088/1742-6596/651/1/012001.

[46] G. T. Zatsepin and V. A. Kuzmin. Upper limit of the spectrum of cosmic rays. *JETP Lett.*, 4:78–80, 1966. [Pisma Zh. Eksp. Teor. Fiz.4,114(1966)].

[47] Kenneth Greisen. End to the cosmic-ray spectrum? *Phys. Rev. Lett.*, 16:748–750, Apr 1966. doi: 10.1103/PhysRevLett.16.748. URL `http://link.aps.org/doi/10.1103/PhysRevLett.16.748`.

[48] Karen Salomé Caballero Mora. Identifying the nature of high energy astroparticles. *Journal of Physics: Conference Series*, 761(1):012077, 2016. URL `http://stacks.iop.org/1742-6596/761/i=1/a=012077`.

[49] Diego Harari. Ultra-high energy cosmic rays. *Phys. Dark Univ.*, 4:23–30, 2014. doi: 10.1016/j.dark.2014.04.003.

[50] R. U. Abbasi et al. Pierre Auger Observatory and Telescope Array: Joint Contributions to the 34th International Cosmic Ray Conference (ICRC 2015). 2015.

[51] Todor Stanev. Ultra high energy cosmic rays. *eConf*, C040802:L020, 2004.

[52] Enrico Fermi. On the Origin of the Cosmic Radiation. *Phys. Rev.*, 75:1169–1174, 1949. doi: 10.1103/PhysRev.75.1169.

[53] A. M. Hillas. The Origin of Ultrahigh-Energy Cosmic Rays. *Ann. Rev. Astron. Astrophys.*, 22:425–444, 1984. doi: 10.1146/annurev.aa.22.090184.002233.

[54] Martin Land. Dirac monopole from Lorentz symmetry in N-dimensions. I. The Generator extension. 2006.

[55] Manuel Drees. The Top - down interpretation of ultrahigh-energy cosmic rays. *J. Phys. Soc. Jap. Suppl.*, 77B:16–18, 2008. doi: 10.1143/JPSJS.77SB.16.

[56] Nicolas Busca, Dan Hooper, and Edward W. Kolb. Pierre auger data, photons, and top-down cosmic ray models. *Phys. Rev.*, D73:123001, 2006. doi: 10.1103/PhysRevD.73.123001.

[57] D. V. Semikoz. Constraints on top-down models for the origin of UHECRs from the Pierre Auger Observatory data. 4:433–436, 2007. URL `http://lss.fnal.gov/cgi-bin/find_paper.pl?conf-07-375`. [4,433(2007)].

[58] Alexander Aab et al. Search for photons with energies above 10^{18} eV using the hybrid detector of the Pierre Auger Observatory. *Submitted to: JCAP*, 2016.

[59] F. Aharonian. Primary particle acceleration above 100 TeV in the shell-type Supernova Remnant RX J1713.7-3946 with deep H.E.S.S. observations. *Astron. Astrophys.*, 464:235–243, 2007. doi: 10.1051/0004-6361:20066381.

[60] F. Aharonian et al. A detailed spectral and morphological study of the gamma-ray supernova remnant rx j1713.7-3946 with h.e.s.s. *Astron. Astrophys.*, 449:223–242, 2006. doi: 10.1051/0004-6361:20054279.

[61] T. P. Li and Y. Q. Ma. Analysis methods for results in gamma-ray astronomy. *Astrophys. J.*, 272:317–324, 1983. doi: 10.1086/161295.

[62] F. Aharonian et al. The Crab nebula and pulsar between 500-GeV and 80-TeV. Observations with the HEGRA stereoscopic air Cerenkov telescopes. *Astrophys. J.*, 614:897–913, 2004. doi: 10.1086/423931.

[63] A. U. Abeysekara et al. Observation of the Crab Nebula with the HAWC Gamma-Ray Observatory. *arXiv*, 1701.01778, 2017.

[64] Grigory Rubtsov, Petr Satunin, and Sergey Sibiryakov. On calculation of cross sections in Lorentz violating theories. *Phys. Rev.*, D86:085012, 2012. doi: 10.1103/PhysRevD.86.085012.

[65] M. Schreck. Vacuum Cherenkov radiation for Lorentz-violating fermions. *arXiv*, 1702.03171, 2017.

[66] H. Martínez-Huerta and A. Pérez-Lorenzana. Vacuum Cherenkov radiation and photon decay rates from generic Lorentz Invariance Violation. *J. Phys. Conf. Ser.*, 761(1):012035, 2016. doi: 10.1088/1742-6596/761/1/012035.

[67] H. Martínez-Huerta and A. Pérez-Lorenzana. Photon emission and decay from generic Lorentz Invariance Violation. *J. Phys. Conf. Ser.*, 866(1):012006, 2017. doi: 10.1088/1742-6596/866/1/012006.

[68] A. Aab et al. Depth of maximum of air-shower profiles at the Pierre Auger Observatory. II. Composition implications. *Phys. Rev.*, D90(12):122006, 2014. doi: 10.1103/PhysRevD.90.122006.

[69] *The Pierre Auger Observatory: Contributions to the 34th International Cosmic Ray Conference (ICRC 2015)*, 2015. URL `http://inspirehep.net/record/1393211/files/arXiv:1509.03732.pdf`.

[70] R. U. Abbasi et al. Pierre Auger Observatory and Telescope Array: Joint Contributions to the 34th International Cosmic Ray Conference (ICRC 2015). 2015.

[71] Douglas R. Bergman. Observation of the GZK Cutoff by the HiRes Experiment. In *Proceedings, 30th International Cosmic Ray Conference (ICRC 2007): Merida, Yucatan, Mexico, July 3-11, 2007*, volume 4, pages 451–454, 2007. URL `http://indico.nucleares.unam.mx/contributionDisplay.py?contribId=1128&confId=4`.

[72] Alessandro De Angelis, Giorgio Galanti, and Marco Roncadelli. Transparency of the Universe to gamma rays. *Mon. Not. Roy. Astron. Soc.*, 432:3245–3249, 2013. doi: 10.1093/mnras/stt684.

[73] Giovanni Amelino-Camelia. On the fate of Lorentz symmetry in relative-locality momentum spaces. *Phys. Rev.*, D85:084034, 2012. doi: 10.1103/PhysRevD.85.084034.

[74] J. M. Carmona, J. L. Cortés, and B. Romeo. Modified energy–momentum conservation laws and vacuum Cherenkov radiation. *Astropart. Phys.*, 71:21–30, 2015. doi: 10.1016/j.astropartphys.2015.04.009.

[75] Rodrigo Guedes Lang, Humberto Martínez-Huerta, and Vitor de Souza. Limits on the Lorentz Invariance Violation from UHECR astrophysics. *arXiv*, 1701.04865, 2017.

[76] C. Patrignani et al. *Chin. Phys. C*, 40:100001, 2016. Particle Data Group.

[77] Don Colladay and V. Alan Kostelecky. CPT violation and the standard model. *Phys. Rev.*, D55:6760–6774, 1997. doi: 10.1103/PhysRevD.55.6760.